Stony Brook University

An Ambient and Surfactant-less Synthesis of Segmented Palladium/Gold Multi-functional Nanowires

A Thesis Presented

by

Zhibo Tan

to

The Graduate School

in Partial Fulfillment of the

Requirements

for the Degree of

Master of Science

in

Chemistry

Stony Brook University

December 2012

Stony Brook University

The Graduate School

Zhibo Tan

We, the thesis committee for the above candidate for the

Master of Science degree, hereby recommend

acceptance of this thesis.

Thesis Adviser

Stanislaus S. Wong
Professor, Department of Chemistry

Second Reader

Michael G. White
Professor, Department of Chemistry

Third Reader

Joseph W. Lauher
Professor, Department of Chemistry

This thesis is accepted by the Graduate School

Charles Taber
Interim Dean of the Graduate School

Abstract of the Thesis

An Ambient and Surfactant-less Synthesis of Segmented Palladium/Gold Multi-functional Nanowires.

by

Zhibo Tan

Master of Science

in

Chemistry

Stony Brook University

2012

Abstract: Segmented noble metal nanowires (NWs) represent an exciting, multifunctional one-dimensional structural architecture with a variety of potential applications. However, currently available methodologies for preparing these systems require either rigorous reaction conditions or expensive equipment. An example of such a conventional protocol is electrodeposition. These strict requirements have limited the potential for these systems to be produced on a large scale, since this protocol is costly and requires complex processes and caustic reaction media. Given the inherent limitations of such methodologies, we report for the first time an ambient, surfactantless template-based approach for the reliable production of Pd/Au segmented nanowires that is not only sustainable but also efficient. Our simple two-step synthetic approach allows for direct and predictable control over the relative segment lengths in these nanomaterials. Moreover, thorough structural characterization of these as-prepared samples confirms that our segmented nanowires maintain high quality, crystalline, elementally pure subunits with a well-defined interface between the constituent metals. In the context of preparing segmented nanowires as multifunctional nanostructures, we demonstrate that these as-prepared nanowires achieve high levels of performance when employed as both electrocatalysts and nanomotors.

Table of Contents

List of Figures

highlight the polycrystalline texture at the site of initial Pd nucleation (B), the nearly single crystalline texture of the Pd near the interface between the subunits (C), and the polycrystalline nature of the particular Au segment (D).

37 **Figure 9.** EDAX map of the combined Pd and Au-L edge signals (A) and HAADF (inset) data are shown of the interfacial region between the Pd and Au segments of a representative Pd/Au segmented NW. EDAX maps separately highlighting the Au edge signal (B) and Pd signal (C) are also shown. The intensities of the Pd and Au EDAX signals are plotted (D) as a function of the spatial position across the interfacial region.

40 **Figure 10.** Cyclic voltammograms obtained from Pd/Au nanowires (A) and elemental Pd nanowires (B) obtained in deoxygenated 0.1 M $HClO_4$.

42 **Figure 11.** CO stripping voltammograms associated with Pd/Au nanowires (A) and with elemental Pd nanowires (B) obtained in deoxygenated 0.1 M $HClO_4$.

43 **Figure 12.** Polarization curves (anodic sweep direction) obtained from Pd/Au nanowires (blue) and elemental Pd nanowires (black) in an oxygen-saturated 0.1 M $HClO_4$ solution at 1600 rpm and 20°C. The measured surface activity normalized kinetic currents (specific activities) at 0.9 V are shown as an inset.

47 **Figure 13.** The velocity of Pd/Au nanowires dispersed into an aqueous solution as a function of the concentration of H_2O_2 present. The region between 0 and 1 M is expanded for the sake of clarity and shown as an inset.

49 **Figure 14.** Graphical depiction of the 2D trajectory (measured by confocal microscopy), traced out by Pd/Au nanowires in 9 M H_2O_2 (black trace) and pure water (red). The nanowire motion is captured over a period of 20 s with the initial position ('t' = 0 s) of the nanowire, arbitrarily placed at (0, 0).

List of schemes

List of Equations

List of Abbreviations (Alphabetical)

Full terminology	**Abbreviation**
Zero-dimensional	0D
One-dimensional	1D
Two-dimensional	2D
Three-dimensional	3D
Adenosine triphosphate	ATP
Gold	Au
Carbon monoxide stripping	CO stripping
Cyclic voltammetry	CV
Dichloromethane	DCM
De-ionized water	DI water
Energy dispersive X-ray spectroscopy	EDAX
Electrochemically accessible surface area	ESA
Face-centered cubic	FCC
Glassy carbon rotating disk electrode	GCR-DE
Hydrogen peroxide	H_2O_2
High angle annular dark field image	HAADF image
Hydrogen adsorption and desorption	H_{ads}
Tetrachloroauric acid	$HAuCl_4$
Perchloric acid solution	$HClO_4$
High resolution transmission electron microscope	HR-TEM
Isopropyl alcohol	IPA

Methanol oxidation reaction	MOR
Hexachloropalladate hydrate	Na_2PdCl_6
Sodium borohydride	$NaBH_4$
Nanowire	NW
Optical-reflective microscope	ORM
Oxygen reduction reaction	ORR
Polycarbonate template	PC template
Palladium	Pd
Polymer electrolyte membrane fuel cells	PEMFCs
Platinum	Pt
Physical vapor deposition	PVD
Rotating disk electrode method	RDE
Reversible hydrogen electrode	RHE
Selected area electron diffraction	SAED
Scanning electron microscope	SEM
International system of units	SI
Solution-liquid-solid	SLS
Transmission electron microscope	TEM
Ultra violate-visible spectroscopy	UV-visible
Vapor-liquid-solid	VLS
X-Ray diffraction	XRD

Acknowledgements

Research (including support for SSW) was supported by the U.S. Department of Energy, Basic Energy Sciences, Materials Sciences and Engineering Division. The author greatly appreciates the efforts exerted by Mr. Christopher Koenigsmann, who contributed to the philosophical underpinning of this idea as well as by Mr. Jared Jacobskind and Ms. Huiqing Peng, who both have devoted significant time to the experimental development of this study. The author also thanks Dr. Eli Sutter for her assistance with obtaining the HR-TEM-SAED measurements, Dr. J. Quinn for assistance for help with the SEM-EDAX measurements, and Dr. Radoslav Adzic (Brookhaven National Laboratory) for facilitating the electrochemical measurements. We also acknowledge Dr. GuoWei Tian and the Central Microscopy Imaging Center (CMIC) at Stony Brook University for help with the confocal microscopy data. Experiments were performed in part at the Center for Functional Nanomaterials located at Brookhaven National Laboratory, which is supported by the U.S. Department of Energy under Contract No. DE-AC02-98CH10886.

Chapter I. Introduction

What is Nano? Nano is an SI prefix denoting a factor of 10^{-9}. It is derived from the Greek term νᾶνος, meaning dwarf. It is most frequently used in defining lengths, which is symbolized as a lower case letter "n". In the field of nanotechnology, the context of "nano" is adopted length-wise in order to define materials that are smaller than 10^{-6} meter. Figure 1 illustrates the scale between a nanomaterial and some everyday materials.

Figure 1. Schematic illustration of the scale of nanomaterials vs. macroscale objects. Acquired from the National Nanotechnology Initiative (www.nano.gov).

Nanomaterials come in many shapes and sizes, but are generally categorized by how many dimensions are confined to the nanoscale. These are denoted as either a zero-dimensional (0D), one-dimensional (1D), two-dimensional (2D), or three-dimensional (3D) nanomaterial, respectively. Nanoparticles, quantum dots, and many other nanomaterials, that do not possess any dimension greater than 100 nm, are categorized as 0D nanomaterials. Nanowires and nanotubes, as denoted by their names, tend to exceed their longitudinal limitations in only one dimension, and therefore readily fall into the category of a 1D nanomaterial, which possess two dimensions that are quantum constrained to less than 1000 nm. 2D nanomaterials possess only one dimension at the nanoscale, which can be re-defined in terms of nano-scale sheets, which are also known as thin films. 3D nanomaterials can consist of arrays of either 1D nanowires/tubes or micrometer-sized, porous, large-scale aggregates of smaller 0D nanoparticles. These assemblies of smaller nanomaterials can exist on either the millimeter or centimeter scale.

In recent years, enormous attention has been paid to multi-functional nanomaterials, which are composed of subunits within the architecture comprised of diverse functionalities. Examples of such structures include nanoparticles, nanowires, and nanotubes. Amongst these various possibilities, nanowires, which possess the characteristics of only two-dimensionally confined dimensions, demonstrate mechanical robustness with structural flexibility and unique morphological effects,[1-5] and a possible advantage of assembling segments of various materials into one single nanostructure. Amongst various types of multi-functional nanowires, metal nanowires with distinctive optical (including plasmonic),[6,7] electronic,[8] and thermal[9] properties exhibit broader range of applications in bioanalysis[10-16], catalysis[17-21], sensing[22-26], and opto-electronics[10,14,19,22,27,28]. For example, our group has devoted a great amount of effort towards developing Pd, Pt, Au, and Ru nanowires[5,29-35] with a recent emphasis on highlighting

improvements in designing electrocatalyts towards the oxygen reduction (ORR) and alcohol oxidation reactions, which are essential for use in low-temperature polymer electrolyte membrane fuel cells (PEMFCs).[32,36,37]

Based upon our previous studies, we expanded our investigation into the development of a nanowire system that incorporates and/or fuses different metals as constituent components of a completely inclusive, seamless architecture. Specifically, we have been aiming at merging the favorable properties of several individual metals into an integral whole, whose subunit properties are individually conserved but whose sum functionality could be inherently better than its separate components. Alloyed nanowires, in general, demonstrate enhanced overall performance. However, alloying of metals leads to a composite material with electronic and structural properties that are drastically different from the individual component metals. In order to integrally preserve the elemental property of each component, we need to prevent a high degree of mixing between each metallic element.

Segmentation of a nanowire provides a solution towards resolving the above-mentioned concerns. A multi-segmented metal nanowire is composed of multiple, diverse segments of elements, alloys, or a combination of both types of metals within a discrete structure. This strategy has the potential to enhance individual segmental performance through cooperative effects.[38-40] Furthermore, segmentation of metals with differing optical reflectivity properties allows for the subunits to arrange themselves into unique sequences, thereby producing a "bar-coded" type material with potentials in applications such as sequencing[10,11] and electronic memory-formation.[19]

In addition, segmented metal nanowires are known for exhibiting chemotaxis behaviors in the presence of appropriate stimuli. Chemotaxis, in a biological context, is defined as "the

movement of organisms either towards or away from a particular chemical attractant or toxin through a biased random walk process."[41] Biological nanomotors commonly use adenosine triphosphate (ATP) as the energy source, converting chemical energy into mechanical forces, which translates into locomotion. Based upon this unique property, kinesins and dyneins, for example, have been well studied and applied as artificial transporters in order to relocate cargo including proteins and DNA within a living organism.[42-45] Nevertheless, the fuel source for these above-mentioned biological nanomotors is rarely available outside of a biological system. As such, non-biological materials that mimic chemotaxis behavior possess great potential towards the development of an artificial nanoscale self-regulated transporting system. The key attribute of these asymmetrically designed nanomotors is their capability for converting chemical energy into autonomous, non-Brownian motion in low-ionic strength aqueous solutions.[46] The literature demonstrates a wide variety of bi-metallic nanomotors[2,41,42,44-65] that take advantage of this potential for a variety of applications. For example, a nanowire can load up a "cargo" molecule, transport it across a concentration gradient and subsequently unload the cargo at the designated location.

In considering the above-mentioned advantages and applications' potential, we have dedicated our focus of research upon multi-functional materials in order to develop a multi-segmented metal nanowire system.

The component ratio of the constituents of the nanowire is essential to the overall property of the multi-segmented nanostructure. Specifically, a longer subunit can potentially lead to an amplification of effects related to that particular metal element. Therefore, quantitatively manipulating the relative lengths of the various subunits represents a powerful method for tailoring the properties of these nanomaterials.[66] For instance, coupling the uniquely

advantageous flexibility of this structural architecture with the highly favorable optical, electronic, and catalytic properties of noble metals has rendered this class of segmented materials as excellent candidates for a broad range of applications including but not limited to sensors,[10,14] bio-analysis,[11,39] nanomotors,[2,41,42,44-64] colloidal transport,[22,54] catalysis,[67-69] and nano-electronics.[70]

The traditional synthetic methodologies for nanowires where control over the length is retained readily fall into two categories, namely top-down and bottom-up approaches.[71] The top-down approach often utilizes a lithography technique in combination with a chemical etching process in order to obtain nanoscale materials from a wasteful quantity of starting precursors.[72] This method has limitations in terms of the size and chemical composition of nanowires produced and is often not only costly but also resource intensive. The bottom-up approach assembles the smallest building blocks into functional nanowires, which are relatively less expensive and efficient. One classical strategy for the bottom-up approach incorporates the use of catalysts in order to direct 1D nanowire growth, a protocol which can be divided into both vapor-liquid-solid (VLS)[73] growth and solution-liquid-solid growth (SLS)[74] methods, based on the phase involved in the reactions. Currently, most of the precisely-controlled nanowire growths are accomplished by VLS methods, including chemical vapor deposition[75], thermal evaporation[76], laser ablation,[77] and many similar variations. The VLS method can precisely control the nanowire length by manipulating the deposition rate and duration. In addition, it also can be used to introduce specific segments by simply changing the precursors required for deposition. However, these methods are still costly, due to the requirement of rigorous reaction conditions such as high temperature and pressure, complex synthetic equipments including an external power source, and the presence of preformed growth catalysts. Therefore, in essence, the VLS

method has a low efficiency in respect to its requirements and costs.

Another straightforward route towards synthesizing metal nanowires involves template-based synthesis.[78-80] The use of either a surfactant or a physically confining template, including carbon nanotubes and porous membranes, is a conceptually simpler process and has been widely applied to the synthesis of various types of nanowires.[71] Specifically, the porous structure within the template provides empty space for the metal to nucleate and grow into a nanostructure that occupies and hence resembles the morphology of the occupied porous space.

Electrodeposition, coupled with template synthesis, is popular because it has the capability of not only controlling the length but also the composition of nanowires by manipulating the deposition voltage and the deposition precursor solution. This method is physically simpler and relatively more cost-effective than the VLS method. Nevertheless, prior to the actual nanowire growth, the porous template, which will be used as the scaffold, must first be plated with a thin metal layer on one side of the template surface in order to serve as the working electrode as well as a physical boundary to the nanowire extension through costly and complex processes such as physical vapor deposition (PVD). This PVD-deposited additional metal layer is typically not a component of the desired nanowire system and therefore it must be removed by later processes. This extra plating hence not only is a waste of resources but also necessitates a high requirement on the associated preparation conditions such as the need for high vacuum and high temperature. Moreover, the electrodeposition process involves the use of an external power supply to generate electric current for the redox reactions on the two electrodes, an ionic solution serving as the electrolyte, and the careful control of current flow. Overall, this synthesis process is not only energy consuming but also the ionic solution utilized is normally acidic and therefore not environmentally friendly. These above-mentioned limitations of this method render

electrodeposition less suitable for application in the mass production of nanowires.

Therefore, a key endeavor in the processing of practical multi-segmented nanowires has been to employ ambient, solution-based techniques that can be performed in neutral solution without the need for a separately prepared electrode or for any additional power sources. In this context, we have chosen herein to embark upon the controlled synthesis of segmented nanowires in a polycarbonate (PC) template using an ambient and surfactant-less U-tube double diffusion method. This method employs a U-shaped double half-cell device and a selected PC template as the reaction chamber for nanowire growth (Scheme 1).

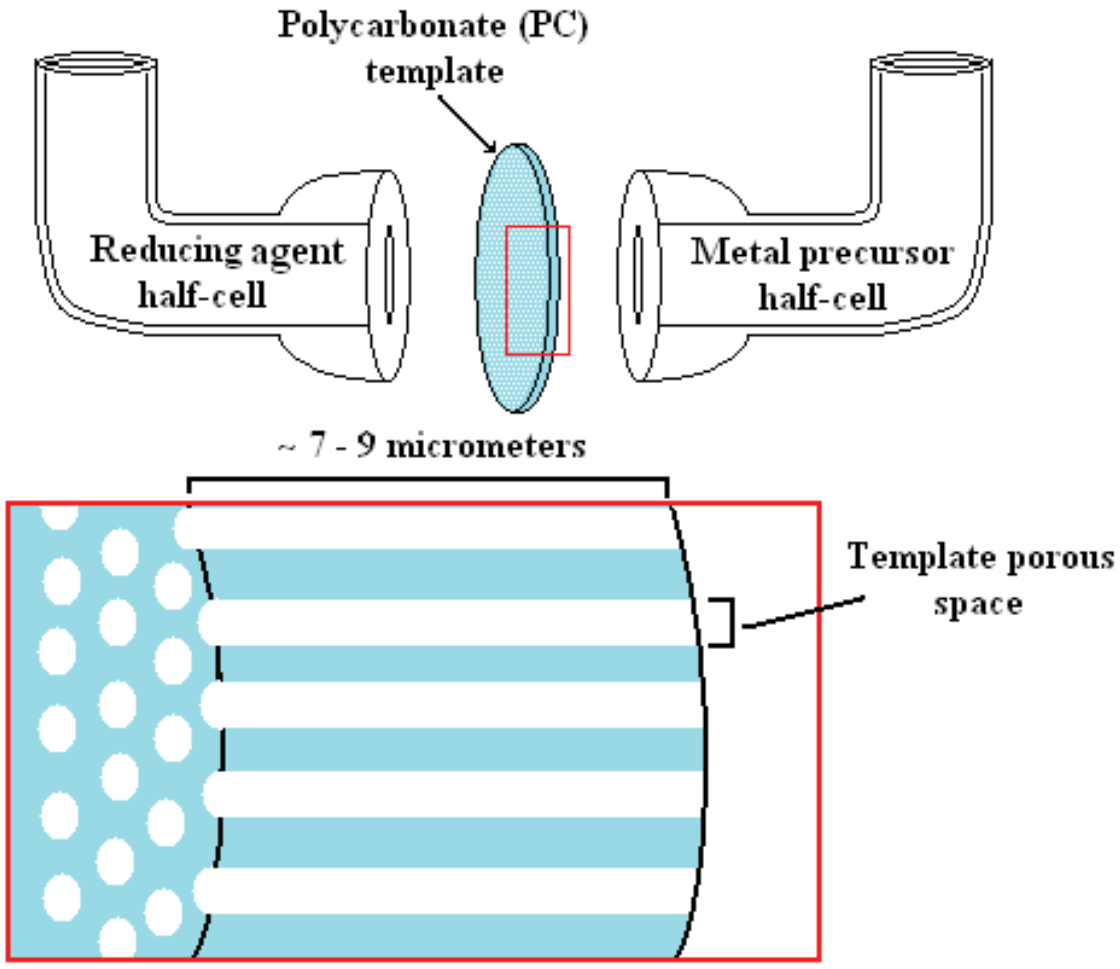

Scheme 1. U-tube double diffusion device with a selected PC template.

This protocol allows metal precursors to be reduced within the template by the reducing agent, without a need for an additional electron source. Previous studies utilizing the U-tube method for the synthesis of elemental and alloyed metal nanowires[5,29-32,34,35,38,81,82] have confirmed that this method is not only efficient but also environmentally friendly for the production of high-quality single crystalline nanowires under ambient conditions. The mechanism of this U-tube method is simple: the metal precursor and the reducing agent are placed in the U-tube half-cells and are physically separated by the PC template. Both of the solutions gradually diffuse into the porous spaces within the PC template at various rates. Upon contact, the reducing agent reduces the metal procures, hence lead to metal nucleation.

Under double diffusion conditions, the growth of nanowires is dependent on the concentration of both reagents, as well as the diameter of the pore.[5,29-32,34,35,38] With either relatively high reagent concentrations or smaller pore diameter, the fronts of both reagents would diffuse at similar rates, resulting in an initiation of nucleation at the central region of the porous space and subsequent nucleation in both directions. With relatively large pore diameters, the nucleation process initiates throughout the entire porous spaces, resulting in nanowire formation across the entire pore volume. Neither of the above mentioned conditions can be suitability applied for segmented nanowire growth. Fortunately, prior studies of elemental palladium (Pd) nanowire growth[31] has demonstrated a completely different growth mechanism that is particularly suitable for segmented nanowire growth. With a large diameter porous space and relatively low reducing agent concentration, Pd can initiate the nucleation process at the interface between the template surface and the reducing agent, which is then followed by a uni-directional nanowire growth. This unique initial process can lead to the formation of a thin layer of Pd metal on the external surface of the PC template, exposed to the reducing agent, which functions

analogously as the thin metal layer deposited onto the template surface through the PVD process. The presence of this thin layer of Pd metal on the template surface allows for subsequent reactions to be processed in a manner similar to electrodeposition.

By comparison with the strategy applied in VLS and electrodeposition methods, the segmentation of the U-tube-synthesized nanowires can be achieved by the swapping of the metal precursors. The degree of segregation between segments of a nanowire is essential to the establishment of its potential applications. The most straight-forward method of distinguishing and differentiating between subunits of a highly segregated multi-segmented nanowire is through optical devices such as an optical-reflective microscope (ORM), a scanning electron microscope (SEM) and a high-resolution transmission electron microscope (HR-TEM). A non-optical method such as energy dispersive X-ray spectroscopy (EDAX) can provide quantitative analysis of the degree of segregation between nanowire segments. To establish a well-differentiated multi-segmented nanowire system, we examined a group of optically variant noble metal elements. With regards to its excellent conductivity[83,84] and sensing[85,86] properties, we selected gold (Au) as the candidate for the second subunit on this segmented nanowire system.

With the U-tube double-diffusion method and Pd/Au as the primary objective of this bi-segmented nanowire system, we developed a simple two-step synthesis protocol that can be applied under completely ambient conditions without the need for either toxic chemicals or expensive instrumentation. This methodology has been uniquely advantageous since the relative lengths of the Pd and Au segments can be reproducibly controlled by rationally manipulating the reaction time. Furthermore, we have confirmed that the as-prepared segmented nanowires maintain a well-defined Pd/Au subunit interface along with a high degree of elemental purity with nearly undetectable levels of alloying within each subunit. Both of these important

observations are critical in order to verify that the desirable properties of the individual noble metal subunits are retained in the final multifunctional architecture.

In the context of preparing segmented Pd/Au nanowires as multifunctional nanostructures, we have investigated the performance of our as-prepared nanowires as both electrocatalysts and nanomotors. Cyclic voltammetry (CV) and carbon monoxide (CO) stripping experiments validate the performance of Pd/Au nanowires as electrocatalysts. These experiments further verify that the as-prepared nanowires maintain distinctive, catalytically active Pd and Au surface sites, reflective of the high purity of the elemental subunits. In addition, we also examined the electrocatalytic oxygen reduction performance of the nanowire systems and noted that the Pd/Au nanowires maintain oxygen reduction reaction (ORR) activities of, specifically, 0.27 mA/cm^2, that are commensurate with their elemental analogues, and are consistent with the mutual presence of elemental Pd and Au. These results collectively suggest that the individual, elemental sub-units conserve their distinctive, inherent electrocatalytic properties even when combined into a single segmented nanostructure. Therefore, potentially, these structures have the capacity of behaving as multifunctional catalysts, wherein different constituent components of a single nanowire might feasibly catalyze dissimilar types of reaction, such as ORR and methanol oxidation reaction (MOR), for example.

Spontaneous locomotion observed by our as-prepared Pd/Au nanowires in the presence of H_2O_2 via confocal microscopy demonstrates their potential application in nanoscale transport systems. These results have established that the Pd/Au nanowires maintain velocities of 3.15 μm/s in 9 M H_2O_2, which are three and fold-fold higher than their corresponding velocities measured in distilled H_2O (1.36 μm/s). In addition, the measured velocity of the nanowires can be reliably tuned by manipulating the concentration of H_2O_2 present in solution. Hence, these

results collectively suggest that our template-based approach not only generates high-quality, high-purity, crystalline, segmented nanowires with reliable control over the relative segment length but also serves as a reasonably efficient, simple, scalable, and environmentally benign protocol for producing operationally effective multifunctional nanostructures on a sustainable basis.

Chapter II. Synthesis and Characterizations

2.1. Synthesis of the Pd/Au nanowires.

The Pd/Au nanowires were synthesized in a two-step process involving the growth of an initial metallic Pd nanowire segment followed by the subsequent growth of a second Au layer. This process is described herein.

2.1.1. Synthesis of the Pd subunit.

The synthesis of the Pd nanowire subunit was accomplished through a previously reported template-based U-tube method[31] (Scheme 1). Briefly, a Pd precursor and a reducing agent solution consisting of 50 mM sodium hexachloropalladate hydrate ($Na_2PdCl_6 \cdot xH_2O$, 99.9%, Alfa Aesar) and 5 mM sodium borohydride ($NaBH_4$, 98%, Acros) were prepared, respectively. The Pd chemical reduction process in an acidic solution (1 M H^+) is shown as Equation 1.[87] The reduction process in an ethanolic environment is expected to be similar in nature.

Equation 1: Reduction of Pd precursor in aqueous under acidic conditions.

$$PdCl_6^{2-} + 4\ e^- \leftrightarrow Pd + 6\ Cl^- \qquad 0.9395\ E°/V$$

Immediately prior to synthesis, the internal one-dimensional pores of a 200 nm PC membrane (Whatman, Nucleopore track-etched) were saturated by briefly sonicating the membrane in ethanol. After sonication, the PC membrane, serving as a template for the growth of the nanowires, was mounted between the two glass half-cells of the U-tube double diffusion device while subsequently being clamped tightly for leakage prevention. The reaction was initiated by the simultaneous addition of the precursor and reducing agent solutions into the two respective half cells. Pd nucleation could be visually confirmed by the formation of a layer of shiny metallic material on the external surface of the template, exposed to the reducing agent half-cell. Utilizing this observation as a reference point, the reaction of the Pd segment was

allowed to proceed with times varying from 4 – 86 min, producing Pd nanowire segments with corresponding lengths ranging from 1 – 6 μm, respectively. To terminate the reaction, both the Pd precursor and reducing agent were rapidly removed from the half-cells simultaneously, thereby quenching the growth of the Pd nanowire segment. Subsequently, aliquots of ethanol were added into the half-cells and kept in solution for 5 minutes, in order to remove residual traces of Pd precursor and reducing agent from the template pores.

2.1.2. Synthesis of the Pd-based Au segment.

Following the synthesis of the as-prepared Pd nanowire subunit, an Au segment was grown from the existing Pd nanowire subunit, via a similar electroless deposition process. Specifically, after removal of the ethanol wash from the first step, the precursor and reducing half-cells were loaded with a 50 mM tetrachloroauric acid ($HAuCl_4 \cdot xH_2O$, 99.999%, Alfa Aesar) solution and a 100 mM $NaBH_4$ reducing agent solution, respectively. The reduction of Au in an acidic solution (1 M H^+) is shown in Equation 2.[87] The corresponding reduction process in an ethanolic environment is expected to behave similarly.

Equation 2: Reduction of Au precursor in aqueous under acidic conditions.

$AuCl_4^- + 3\ e^- \leftrightarrow Au + 4\ Cl^-$ 1.498 E°/V

The completion of the reaction was signaled by the formation of a thin layer of golden metallic material on the outer surface of the template facing the precursor half-cell. Subsequent removal of the precursor and reducing agent solutions quenched the growth of Au, which indicated the completion of the nanowire synthesis.

2.1.3. Isolation of the Pd/Au nanowires.

To remove the thin metallic layers on external surfaces of the resulting template, gentle polishing was applied on an ethanol-lubricated hard Arkansas whetstone (Best sharpening stones

Inc., 600-800 gt.) until there was a complete removal of the excess metallic material. Subsequently, the PC template containing Pd/Au nanowires was immersed in dichloromethane (DCM, 99.5%, Acros Organics) for 10 minutes to dissolve the PC. Individual nanowires were isolated from the DCM/PC solution by centrifugation at 3000-4000 rpm for 10 minutes. Three additional cycles of DCM immersion and isolation were applied for the purpose of removing residual PC from the suspension. A final product was obtained by dispersing the isolated nanowires into absolute ethanol for further characterization.

For electrochemical measurements, as-prepared Pd/Au nanowires were rendered into catalyst inks by dispersing the individual nanowires into solutions of 25% IPA in water with a concentration of ~2 mg/mL.

2.2. Structural Characterization.

2.2.1. X-Ray diffraction (XRD).

Powder diffraction samples were prepared by dispersing the Pd/Au nanowire samples into ethanol and drop casting the resulting slurry onto a glass microscope slide. Powder diffractograms of as-prepared Pd/Au nanowires were obtained on a Scintag diffractometer, operating in the Bragg-Brentano configuration with Cu Kα radiation (λ = 1.54 Å). Diffraction patterns were collected from 35° to 95° at a scanning rate of 0.2° in 2θ per minute. Slit widths and accelerating voltages were calibrated, based upon the diffractometer standards.

2.2.2. Electron Microscopy

The size, morphology, and chemical composition of the resulting Pd/Au nanowires were initially characterized via a field emission scanning electron microscope (FE-SEM) along with energy dispersive X-ray analysis. Images and spectra were taken on a Leo 1550 SEM instrument at accelerating voltages of 20 kV. Samples were dispersed into ethanol and drop cast onto clean

silicon wafers which were subsequently mounted onto the surfaces of an aluminum holder via conductive carbon tape. High resolution transmission electron microscopy (HRTEM), high angle annular dark field images (HAADF), energy dispersive X-ray data in scanning TEM mode (TEM-EDAX), and selected area electron diffraction (SAED) patterns were acquired on a JEOL 2100F instrument equipped with a Gatan HAADF detector for performing incoherent HAADF / Z-contrast imaging in scanning TEM mode at accelerating voltages of 200 kV with a beam size of 2 Å.

2.2.3. Ultraviolet-visible spectroscopy (UV-visible).

Both Pd and Au have unique UV absorbance peaks, which are revealed by a Beckman Coulter DU 640 UV-visible spectrometer. Pd/Au nanowire samples were well dispersed in ethanol and loaded into a quartz cuvette. Prior to the absorbance collection, a sample with only ethanol was employed as a blank. Subsequently, the Pd/Au nanowires were scanned between 200 and 800 nm at a rate of 240 nm/min.

2.3. Electrochemical Characterization.

Prior to electrochemical experiments, a glassy carbon rotating disk electrode (GC-RDE, Pine instruments, 5 mm) was polished until a pristine finish was obtained. The pristine GC-RDE was pre-modified with a thin carbon layer by rapidly drying two 5 μL drops of a 1 mg/mL solution of Vulcan XC-72R carbon dispersed in 25% IPA so as to improve the dispersion and stability of the Pd/Au nanowire catalysts. Once modified, the GC-RDE was loaded with a single drop of the appropriate catalyst ink, which was allowed to evaporate in air. As-prepared Pd/Au nanowire catalysts were loaded onto the electrode by placing a 5 μL drop of the dispersed catalyst ink onto the surface followed by air drying. Once dry, the various catalyst layers were sealed with a 5 μL drop of a 0.025% Nafion solution prepared by diluting a 5% stock solution

(Aldrich) in ethanol.

Electrochemical measurements were performed in a 0.1 M perchloric acid solution ($HClO_4$), prepared by diluting the acid concentrate (Fisher Scientific, Optima Grade) with high purity water (R = 18.2 MΩ). Platinum foil and an Ag/AgCl (3 M Cl^-) electrode isolated in a double junction chamber (Cypress) served as the counter electrode and reference electrode, respectively. All of the potentials in this paper have been reported with respect to the reversible hydrogen electrode (RHE), unless otherwise specified.

2.3.1. Cyclic Voltammetry (CV).

The measurement of the oxygen reduction reaction (ORR) performance of the various catalyst samples was performed by employing the thin-layer rotating disk electrode method, a protocol recently reviewed in detail by Kocha and co-workers.[88] First, CVs were obtained in deoxygenated electrolyte at a scan rate of 20 mV/s so as to establish the nature of the electrochemically accessible surface area (ESA). The ESA is calculated in this case by converting the average of the hydrogen adsorption and desorption charge (after correcting for the double layer) into a real surface area utilizing the 0.21 μC/cm^2 as a known conversion factor. In the case of as-prepared nanowires, it is important to note that both adsorption and absorption of hydrogen contribute to the measured charge.[30] Therefore, the calculated specific activities within this manuscript represent a lower limit of the potential activity derived from these nanostructures. Furthermore, the gold atoms do not actually undergo hydrogen adsorption and desorption, and thus, the reported ESA is actually related to the presence of Pd active sites as opposed to the entire nanowire surface.[31,89] The ORR activity of the various catalyst samples is measured by obtaining polarization curves in oxygen-saturated electrolytes at 20°C with the electrode rotating at a rate of 1600 rpm and the potential scanned at a rate of 10 mV/s.

2.4. Application of Pd/Au nanowires as Nanomotors.

The precise behavior of Pd/Au nanowire locomotion was visualized and video recorded using a Zeiss LSM 510 META NLO Two-Photon Confocal Microscope at 1000X magnification. The nanowire samples were well dispersed in water immediately before the experiment. Subsequently, the top part of the suspension was loaded onto a ½ inch glass bottom culture dish (MatTek). A corresponding amount of hydrogen peroxide solution (30%, Reagent Grade, BDH) was added to and mixed with the nanowire suspension so as to generate H_2O_2 concentrations ranging from 0.1 to 9 M. The trajectories of at least 10 individual nanowires from each suspension solution were video-recorded with a CCD camera under visible light for 20 seconds each at a rate of 4 images per second with a resolution of 1388 x 1040 pixels. The X and Y coordinates of the individual nanowires were tracked on each frame over the 20 second time period ((X_1, Y_1), (X_2, Y_2), etc.), utilizing the ImageJ software package with the LSM Reader plug-in (National Institute of Health). From these data, the distance traveled as well as the velocity information associated with each nanowire were calculated using Equation 3.

Equation 3. Distance $= \sqrt[2]{(X_2 - X_1)^2 + (Y_2 - Y_1)^2}$

Chapter III. Results and Discussion

3.1. Controlled synthesis of Pd/Au nanowires.

There are two major challenges that appear during the synthesis of multi-segmented nanowires. These, include the precise manipulation of the length of each subunit and maintenance of the purity of each subunit. In the proposed U-tube double diffusion method, the metal precursor and the reducing agent were individually loaded into the two half-cells of the U-tube, which were separated by a PC template (Scheme 1). This PC template possesses one-dimensional porous spaces throughout its thickness, which can be used as the reaction chamber wherein the metallic subunits nucleate. The metal precursor and the reducing agent are expected to diffuse through the pores of the PC template at various speeds. Upon initial contact, the reducing agent immediately reduced the metal precursor and hence initiated the nucleation of the nanowire. Because the template pore spatially confines the nucleation of the metal, the shape of the resulting nanowire is expected to resemble the porous space it occupied within the PC template. Furthermore, this confinement also implied that the maximum achievable length of a nanowire should be equivalent to the total porous space available, which corresponds to the nominal thickness of the PC template.

According to our previous research on synthesizing metal nanowires[31,89] via this demonstrated U-tube double diffusion method, the fronts of the metal precursors and the reducing agent diffuse through the pores at various speeds, a phenomenon which, as we explained previously, was significantly affected by the concentration of both reagents as well as the diameter of the pore. With either relatively high reagent concentrations or smaller pore diameters, the fronts of both reagents would diffuse at a similar rate, thereby resulting in nucleation at the central region of the porous space followed by subsequent nucleation processes

in both directions. This reaction mechanism is suitable for synthesizing both homogeneous elemental nanowires and alloy-type nanowires, which possess uniform chemical composition throughout the entire nanowire structure. For the synthesis of multi-segmented nanowires, however, this mechanism had perceptible shortcomings. Since the initial metal subunit nucleates bi-directionally, the reaction is halted before the first subunit completely occupies the entire porous space, thereby resulting in empty spaces existing at both terminal regions of the pore. As the second metal precursor replaces the first, the second metal subunit will only continue to nucleate at the empty regions localized at the terminal regions, facing the metallic precursor side. Therefore, a shorter first-subunit will necessarily lead to a shorter total length. In other words, multi-segmentation leads to the production of nanowires that may not be able to achieve their maximum length.

Hence, to optimize the multi-segmented nanowire production, we had to overcome the initial challenge of precisely manipulating the nucleation of each subunit. Ideally, the nucleation of the first subunit is expected to initiate at the interface between the pore opening and the reducing agent, followed by nucleation within the pore uni-directionally towards the metal precursor. This nucleation condition is analogous to electrodeposition, which also can lead to growth of nanowires within a template from one surface to another. To accomplish this goal, we conducted a variety of experiments, including introducing a thin layer of gold onto the surface of the template facing the reducing agent via physical vapor deposition, which would serve to completely block the entrance of reducing agent into the porous spaces while maintaining an obvious electron flow pathway and conduit. Although the result of this particular experiment was successful, utilizing this complicated process to deposit the thin layer of gold rendered the entire protocol very costly and hence diminished the effectiveness of the overall performance.

While looking for a substitute protocol, a separate study conducted by our group on metal nanowires inspired an important advance. According to our study on Pd nanowires,[31] in which the U-tube double diffusion method was applied, with smaller pore size PC templates (i.e. 15 nm), the observed Pd nucleation occurred within the central region of the porous space and extended bi-directionally. This phenomenon was in agreement with our previously disclosed reaction mechanism. When utilizing a PC template with a larger pore size (i.e. 200 nm), the result radically differed from the previous experiment, demonstrating that the observed nucleation process was initiated outside of the PC template itself, namely on the surface facing the reducing agent. This observation implied that with wider template pores, the Pd precursor (H_2PdCl_6) would diffuse at a rate higher than the reducing agent's. More interestingly, the initial nucleation resulted in the formation of a short polycrystalline Pd segment within the template pore as well as a thin layer of Pd materials on the exterior surface of the template facing the reducing agent. This Pd layer is believed to serve as the conductive conduit that transfers electrons toward the Pd precursor solution in the interior of the template without the need for an electro-bridge. Moreover, the existence of a thin Pd layer leads to a uni-directional elongation of Pd nanowires towards the Pd precursor.

This result indicates that with 200 nm diameter pore sizes, the initial reduction of the Pd precursor will lead to a result that is chemically equivalent to the formation of a vapor-deposited thin layer of gold described in a previous experiment. This thin Pd layer prevents direct interaction of the precursor and reducing agent while serving as a sufficient conduit for electron transportation. In essence, with a 200 nm PC template system, utilizing the Pd precursor in the initial reaction will guarantee a uni-directional growth of nanowires within the template pores and the attainment of maximum nanowire length. Furthermore, hypothetically, it is possible to

synthesize nanowires of a designated length by simply manipulating the reaction duration. In fact, reaction stoppage can be immediately induced by removal of the metal precursor. In addition, simply substituting the Pd precursor with another metal precursor can lead to the initiation and growth of the second subunit of this segmented nanowire. Hence, this exciting finding suggests an achievable resolution to the first challenge in synthesizing multi-segmented nanowires.

Inspired by this highly advantageous and optimized growth mechanism, a two-step protocol for synthesizing multi-segmented nanowires under ambient, electroless conditions was developed. Scheme 2 demonstrates a detailed synthetic scheme of this two-step protocol.

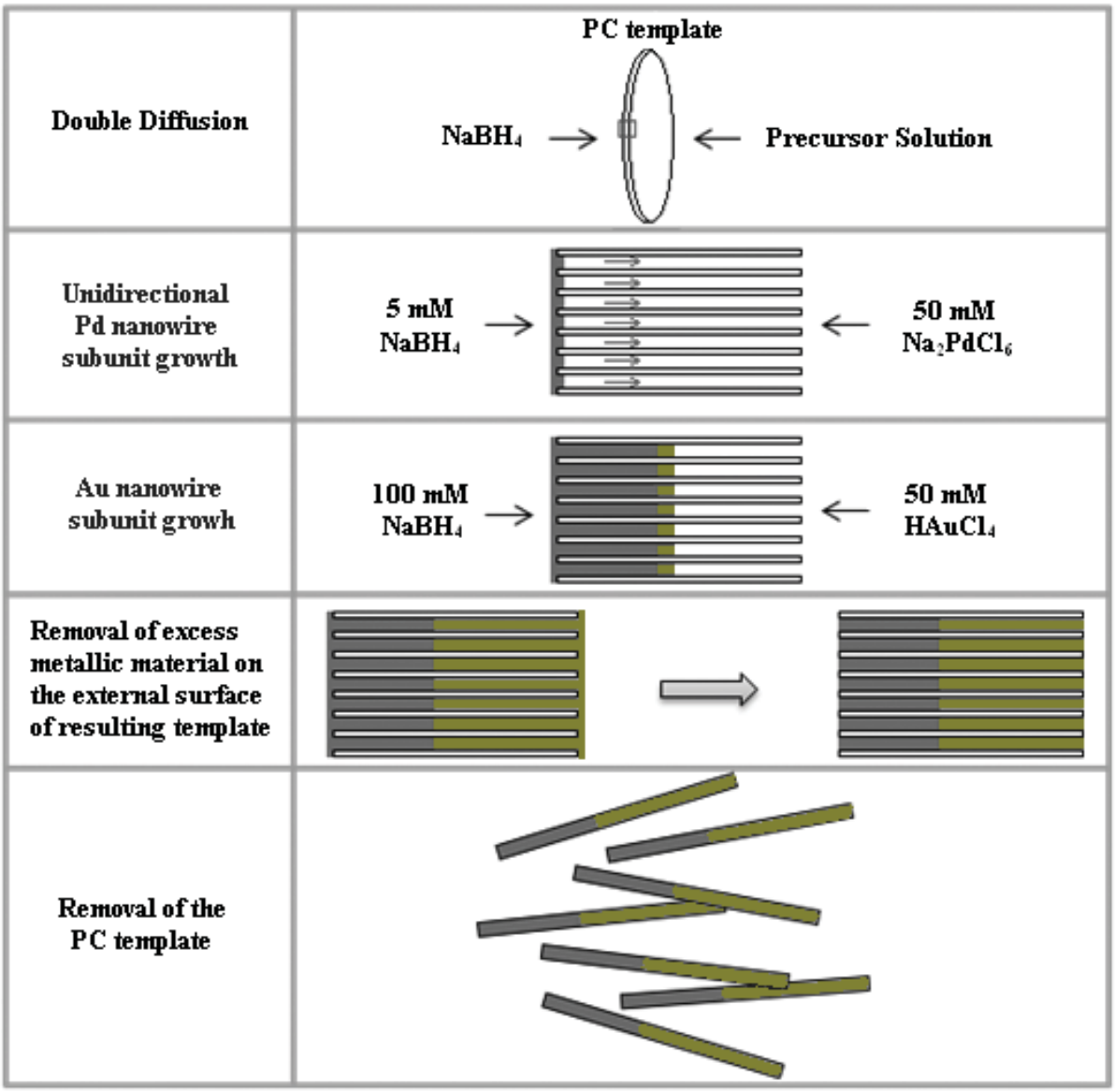

Scheme 2. Schematic of a double-diffusion synthesis of a typical Pd/Au nanowire.

In the first step, a segment of Pd nanowire is grown into the template pore. The initiation of Pd reduction is signaled by the formation of visible metallic material on the exterior surface of the template exposed to the reducing agent. Subsequently, the Pd nanowire elongates towards the half-cell containing Pd precursor until it has achieved the designated length. Upon completion of formation of the first Pd subunit, the Pd precursor and the reducing agent are both removed simultaneously to quench the electroless deposition process.

The second step involves the growth of a second metal, which, in this case, is gold, via another electroless deposition process that continues directly onto the existing Pd subunit. The growth of the Au segment is initiated at the terminal surface of the existing Pd nanowire, which serves as a channel with relatively efficient electron flow that transports electrons from the reducing agent to the unoccupied porous spaces. The Au precursor is then reduced by the flowing electrons. The nanowire therefore continues to elongate towards the area containing Au precursors until the nanowires achieve full occupancy of the pore space and a thin layer of metallic material is formed on the exterior surface of the template exposed to the Au precursor. Upon the completion of Au subunit growth, the template is saturated with the presence of Pd/Au nanowires which occupy the full lengths of the pore spaces.

Noticeably, the reducing agent concentration was significantly different between the first and second reaction (5 mM $NaBH_4$ for Pd reduction versus 100 mM $NaBH_4$ for Au reduction). With a lower reducing agent concentration (5 mM), the initial Pd reduction will occur at a relatively slow rate, which can allow for a more precise control of the Pd subunit length by manipulating the Pd reaction duration. Since the reduction potential of Au is significantly higher than that of Pd, $HAuCl_4$ will galvanically displace Pd metal from the Pd subunit, which necessarily results in the shortening of the existing Pd subunit. Therefore, a significantly higher $NaBH_4$ concentration (100 mM) is required in order to supply a sufficient amount of electrons for Au reduction, which will therefore effectively prevent the galvanic displacement of the existing Pd segment by the gold precursor.

As addressed previously, the Pd subunit length can be easily controlled by manipulating the reaction duration. Longer reaction duration will allow for an increase in crystalline growth and therefore lead to longer Pd subunit lengths. The SEM image confirms that the lengths of the Pd

subunits (Figure 2) systematically increase from 0.94 ± 0.14 μm to 6.68 ± 0.76 μm in an almost linear trend, as the reaction time is increased from 5 to 48 minutes.

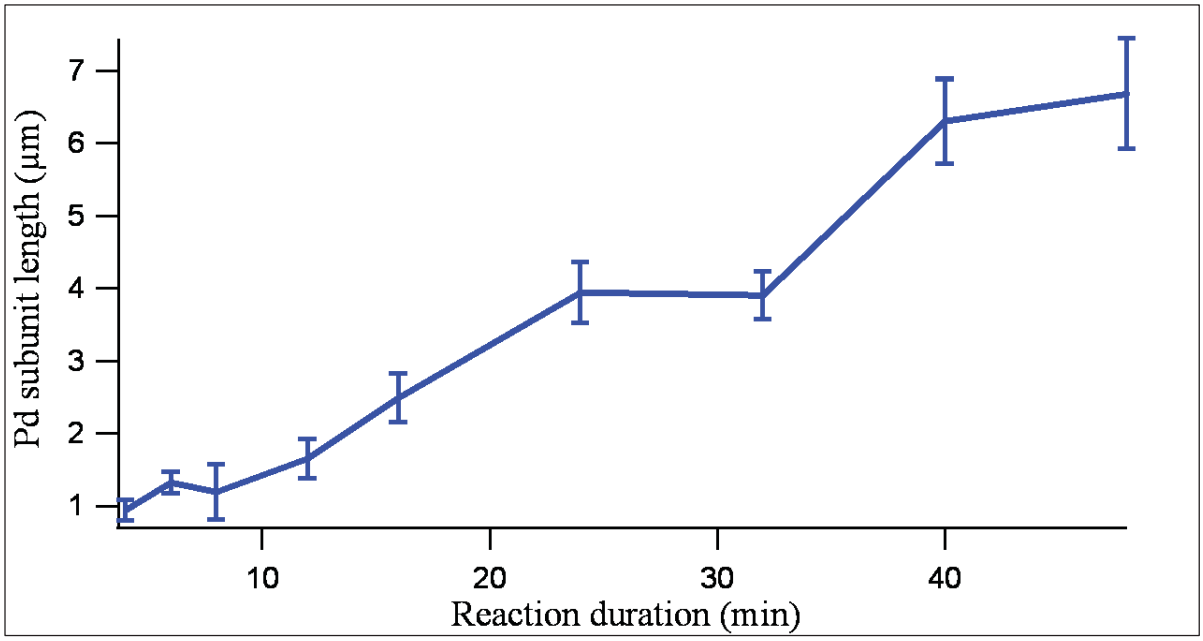

Figure 2. Pd subunit length vs. reaction duration.

Also, both Pd and Au subunits exhibited similar diameters of 260 ± 30 nm, which is in agreement with the pattern of template pore sizes which were previously observed[35,90], and maintained their uniformity during the nanowire growth. This result is not only firmly established within the Pd/Au nanowire system but also in excellent agreement with an analogous Pd/Pt nanowire system[91] as well as with what is known for elemental Pd nanowires.[31] The growth rate of the Au subunit is notably different from that of the Pd subunit, due to the high reducing agent concentration. The high concentration induces the Au subunit to rapidly nucleate throughout the residual unoccupied porous space, i.e. as quickly as 3 min only. Manipulating the subunit length will also result in a corresponding change in the composition ratio. The total lengths of the Pd/Au nanowires are directly dependent on the thickness of the PC template. In this case, our as-synthesized nanowires mostly possess lengths between 7 and 9 μm, which are

analogous to the reported PC template thickness (6-8 μm). With a confined, constant total length, a longer Pd subunit will necessarily result in a relatively shorter Au subunit. Therefore, the ratio of the Au subunit within any Pd/Au nanowire system is complementary to the ratio of the Pd subunit. Figure 3 indicates that the relative length of the Pd subunit increased from 19.97 % to 74.72 % of the total nanowire length, as the reaction time increased from 4 to 48 min. These results validate that the precise manipulation of the subunit length for this multi-segmented nanowire system can be achieved under this completely ambient condition without the need for either electrodeposition or physical vapor deposition.

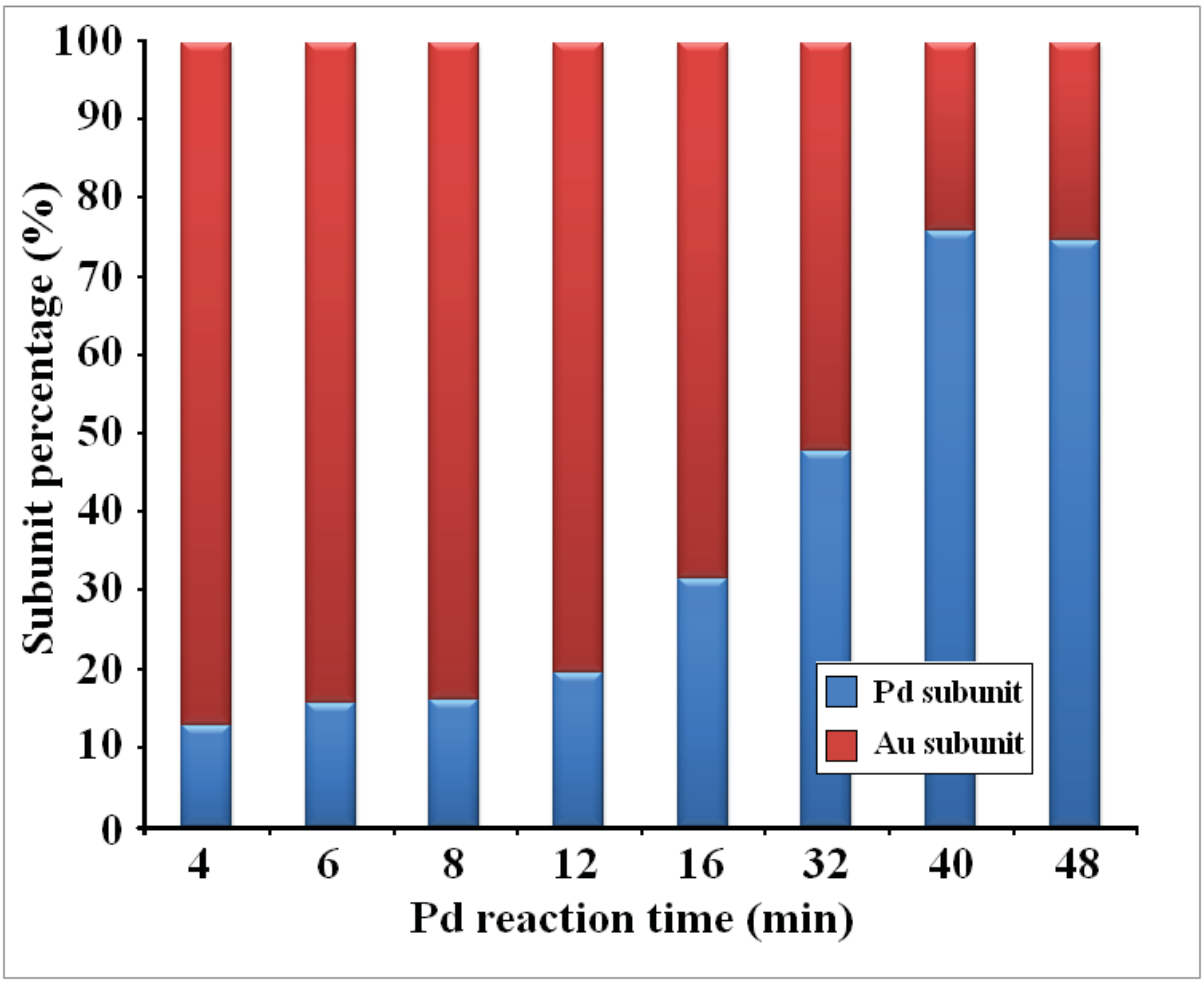

Figure 3. The relative lengths of the constituent nanowire subunits shown as a percentage of the nanowire subunit length with respect to the overall total length of the nanowire as a function of the overall reaction time, utilized in the first reaction step for the generation of Pd/Au nanowires.

3.2. Highly crystalline, non-alloy subunits.

Maintaining the purity and crystallinity of each subunit is another key challenge for synthesizing multi-segmented nanowires. It is not a critical challenge to maintain the purity of the Pd subunit during its initial synthesis, since it is synthesized in the first step after which the U-tubes are thoroughly cleaned. However, the as-synthesized Pd subunit is under threat of being galvanically displaced by the subsequently introduced $HAuCl_4$. The Au subunit, which is

synthesized subsequently to the Pd subunit, poses an issue in terms of maintaining its purity because the half cell previously contained the Pd precursor. The possibility of mixing the residual Pd precursor with the initial Au precursor does exist and could result in the formation of a Pd-Au alloy subunit. To overcome this issue, a 5 min ethanol washing step between precursor loadings was instituted. This washing step will necessarily dilute the residual Pd precursor to a concentration that is significantly and dramatically low as compared with the concentration of the Au precursor. Removal of the washing agents from the half-cells will continue to lower the concentration of the residual Pd precursor. The energy dispersive X-ray spectroscopy (EDAX) data on both Pd and Au subunits (Figure 4) indicate that a high purity elemental structure was achieved for both.

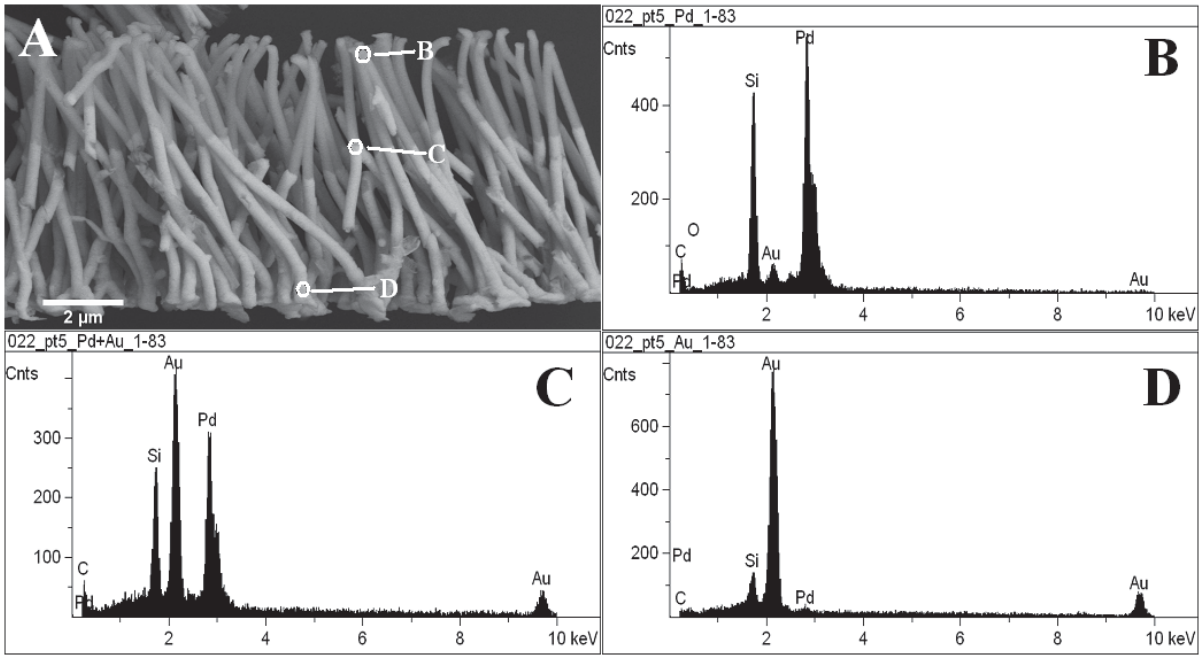

Figure 4. EDAX scan of as-prepared Pd/Au nanowires. A) SEM image of selected nanowires. B) EDAX scan of the Pd subunit. C) EDAX scan of the intersection region between the Pd and Au subunits. D) EDAX scan of the Au subunit. The Si signal originates from the grid.

Specifically, as shown in Figure 4, the EDAX scan of the Pd subunit only detects noticeable

Pd signals (Figure 4b). Complementarily, the scan of the Au subunit reveals that the signal is dominated by the gold L-edge peak. However, some residual nearly undetectable Pd L-edge signal is still present (Figure 4d). The presence of small quantities of Pd representing less than 2 % of the total precious metal content likely arises from residual precursor that remains within the pore space despite the additional ethanol washing. The intersection region of the Pd/Au nanowire maintains characteristics of both subunits, thereby yielding both intensified Pd and Au signals. This result confirms that both Pd and Au subunits maintain a high degree of elemental purity.

To further investigate the purity of our Pd/Au nanowires, we performed power X-ray diffraction on nanowires containing Pd/Au at elemental ratios of 1:3, 1:1, and 3:1 (Figure 5). The diffraction pattern obtained from the nanowires displays peaks, which can be readily indexed to the (111), (200), (220), and (311) planes of pure face-centered cubic (FCC) Pd and Au phases. Also, there are no apparent additional peaks observed in all three individual patterns that could either be attributed to impurities or indicate the presence of a $Pd_{1-x}Au_x$ alloy-type phase.

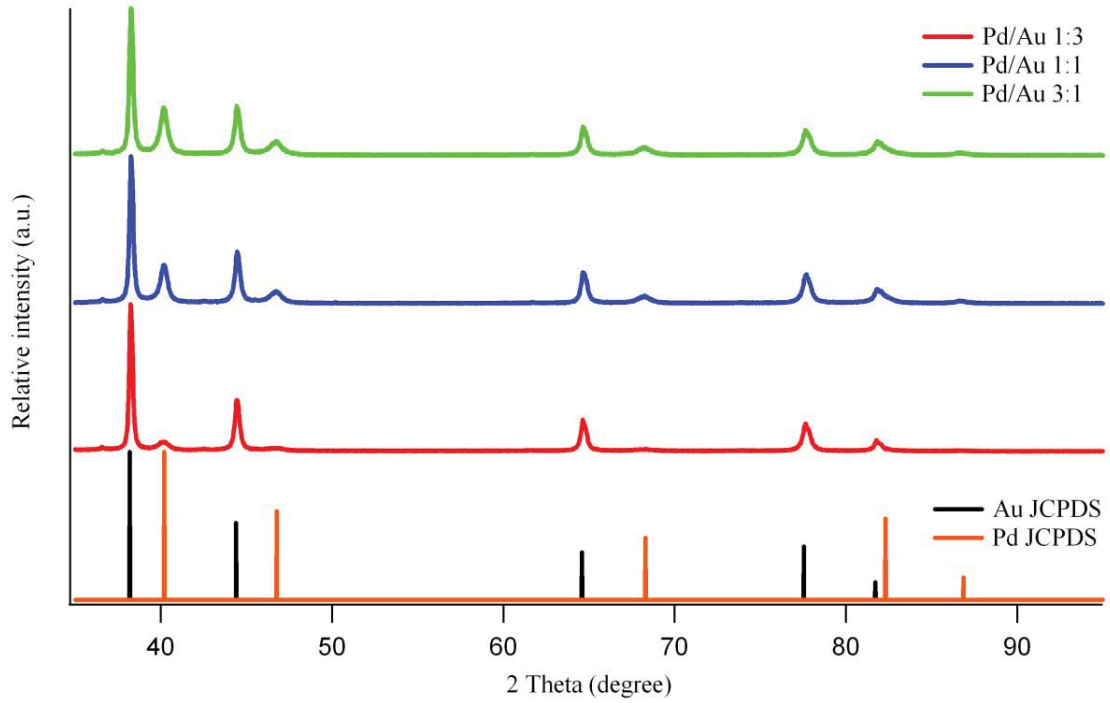

Figure 5. The X-ray diffraction pattern of Pd/Au nanowires with composition ratios of 1:3 (Red), 1:1(Blue), and 3:1(Green). The intensity is shown relative to the measured intensity of the (111) peak.

Furthermore, the expected increment in the relative intensity corresponding to the increase in Au content further confirms that the nanowire composition ratio is directly expressed by the subunit length ratio. These findings collectively suggest that each Pd/Au nanowire is composed of discrete elemental Pd and Au subunits with an absence of alloy-phase impurities.

We have also probed the Pd/Au absorbance through UV-visible (Figure 6) within a 200 nm to 800 nm wavelength range for confirmation of the nanowire composition. With a 1:1 Pd/Au nanowire ratio, there is a noticeable absorbance peak detected at 270 nm with no other apparent peaks being observed. This particular peak agrees with our previous observation on elemental Pd nanowires, which also exhibited significant absorbance in a similar wavelength region. Nevertheless, the expected Au absorbance peak at 560 nm could not be differentiated from the

background. The insert of Figure 6 represents the SEM image of samples prepared for UV-visible spectroscopy, which visually highlights that the nanowires are composed of Pd and Au at an approximately 1:1 ratio.

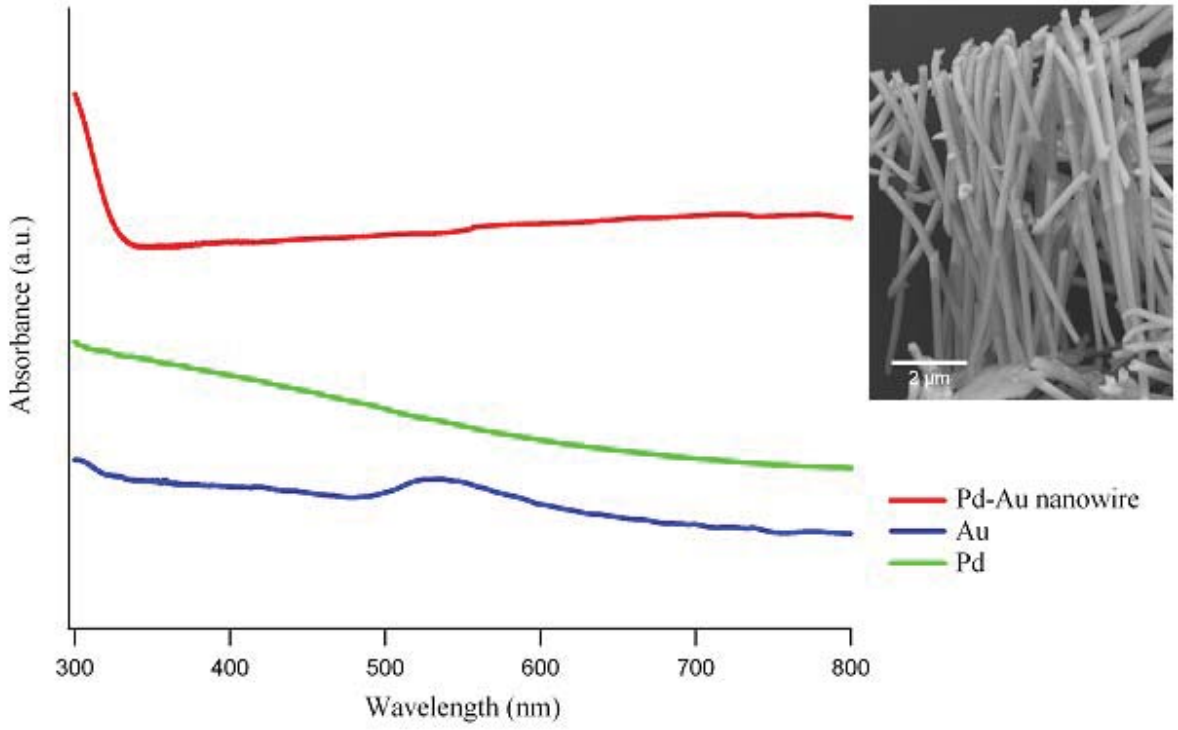

Figure 6. UV-visible spectroscopy absorbance of Pd/Au nanowires with 1:1 composition ratio (Red) and as a comparison, elemental Au nanowires (Blue) and Pd nanowires (Green). Inset: SEM image of as-tested Pd/Au nanowires.

A reasonable explanation for the disappearance of the Au absorbance peak is that Pd, in general, yields a relatively high absorbance throughout the 200 nm to 1000 nm wavelength region. This high scattering background may prevent the effective measurement of the plasmon resonance associated with the elemental gold nanowire. Although our preliminary studies do not demonstrate that the uniquely advantageous optical properties of the Au segment are retained, we believe that further studies such as optical microscopy will clearly show the unique optical properties in our segmented nanowires.

The SEM image of the synthesized Pd/Au nanowires (Figure 7) suggests that they possess subunits which are composed of two distinctively different materials. Figures 7a through 7c represent Pd/Au nanowires with Pd to Au ratios of 1:3, 1:1, and 3:1, respectively. As shown in Figure 7a, the visually brighter segment occupies approximately ¼ of the total nanowire length. In Figures 7b and 7c, the visually brighter segment expands up to ½ and ¾ of the total nanowire length, respectively.

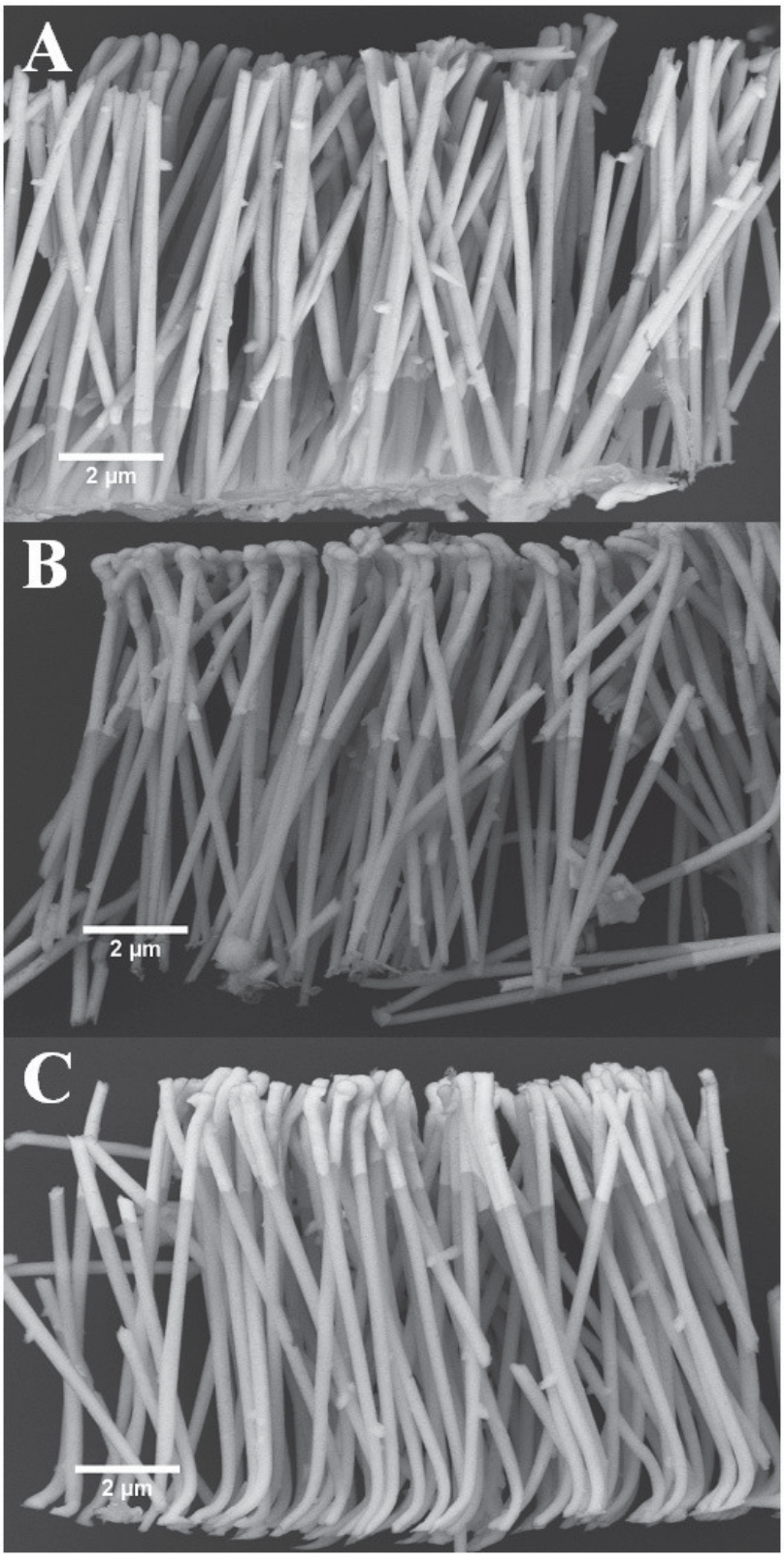

Figure 7. SEM image of Pd/Au nanowires with Pd to Au ratios of 1:3 (A), 1:1 (B), and 3:1 (C).

In consideration of the electron densities of Pd and Au, the visually brighter subunit of the Pd/Au nanowires is expected to be associated with Au, whereas the visually darker subunit is expected to be Pd. The sharp change in contrast at the interface of the Pd and Au sub-units confirms that a well-defined interface is achieved without a significant degree of alloying. In addition, it verifies our ability to precisely manipulate the length of each nanowire subunit.

To complement our examination of the morphology by SEM, we have also employed transmission electron microscopy and selected area electron diffraction to examine both the crystallinity and structure of individual Pd/Au nanowires. The TEM image of a Pd/Au nanowire (Figure 8a) demonstrates distinctive segmentation observed on a Pd/Au nanowire, which is in excellent agreement with the prior SEM data. As shown in Figure 8a, the nanowire is clearly segmented into one dark and one light subunit.

The exhibited SAED result (Figure 8b-d) reveals the crystalline structure of this particular Pd/Au nanowire. Since the composition of each subunit is known, we can ascertain the directionality of nucleation from Figures 8b to 8d, corresponding to the respective SAED images.

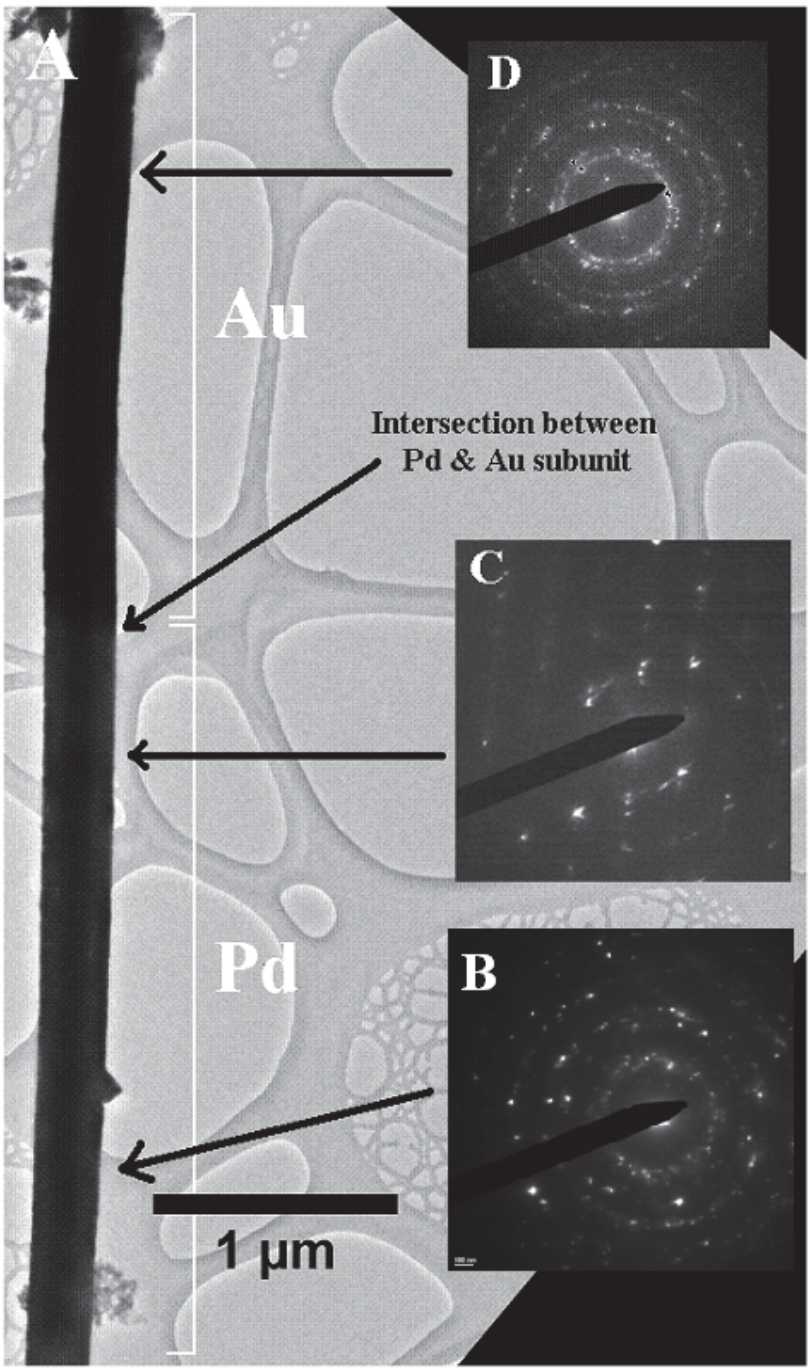

Figure 8. An overview TEM image of a Pd/Au nanowire with the interface between the Pd and Au segments noted (A). The diffraction patterns highlight the polycrystalline texture at the site of initial Pd nucleation (B), the nearly single crystalline texture of the Pd near the interface between the subunits (C), and the polycrystalline nature of the particular Au segment (D).

As shown in Figure 8b, the initial region of the Pd subunit exhibits polycrystalline structure. Similarly, our previous reports on elemental metal nanowires[31] also demonstrate polycrystallinity at the region where nucleation initiates. This phenomenon results from a rapid nucleation process initiated immediately after the Pd precursor solution contacts that of the 5 mM $NaBH_4$ reducing solution. As the nucleation process proceeds, the nucleation speed gradually decreases and leads to a highly oriented crystalline structure (Figure 8c), which is completely in agreement with our previous studies.

The Au subunit maintains a polycrystalline structure throughout the entire length (Figure 8d), mainly due to the higher reaction rate used to form it. As stated in the previous section, 100 mM $NaBH_4$ was utilized to guarantee a forward-going reduction of $HAuCl_4$. This methodology has been widely applied by our group in the synthesis of a variety of elemental, alloy, and segmented metal nanowires; it effectively prevents erosion of the existing metal structure due to galvanic displacement. Evidently, this Au reduction step proceeds, as expected; it induces a fast nucleation throughout the entire subunit growth process. Therefore, the polycrystalline structure, formed as a result of rapid nucleation steps, is observed throughout the entire Au subunit. The SAED data demonstrate that we can replicate the structure normally obtained by electrodeposition, thereby implying that this electroless synthetic method is capable of reproducing the efficiency of electrodeposition. [92,93] Further investigations will be conducted to produce a more highly ordered crystalline Au structure, based on the idea of reducing the Au subunit growth rate.

A well known advantage of electrodeposition is its capability of producing an immediate compositional conversion at the interface between each subunit. To further analyze and compare the quality of our electroless synthesized Pd/Au nanowires, we have examined the alteration of

the chemical composition at the interface between a Pd and Au subunit through EDAX mapping as well as a line scan (Figure 9) across the subunits' intersection region, which explicitly explores the change.

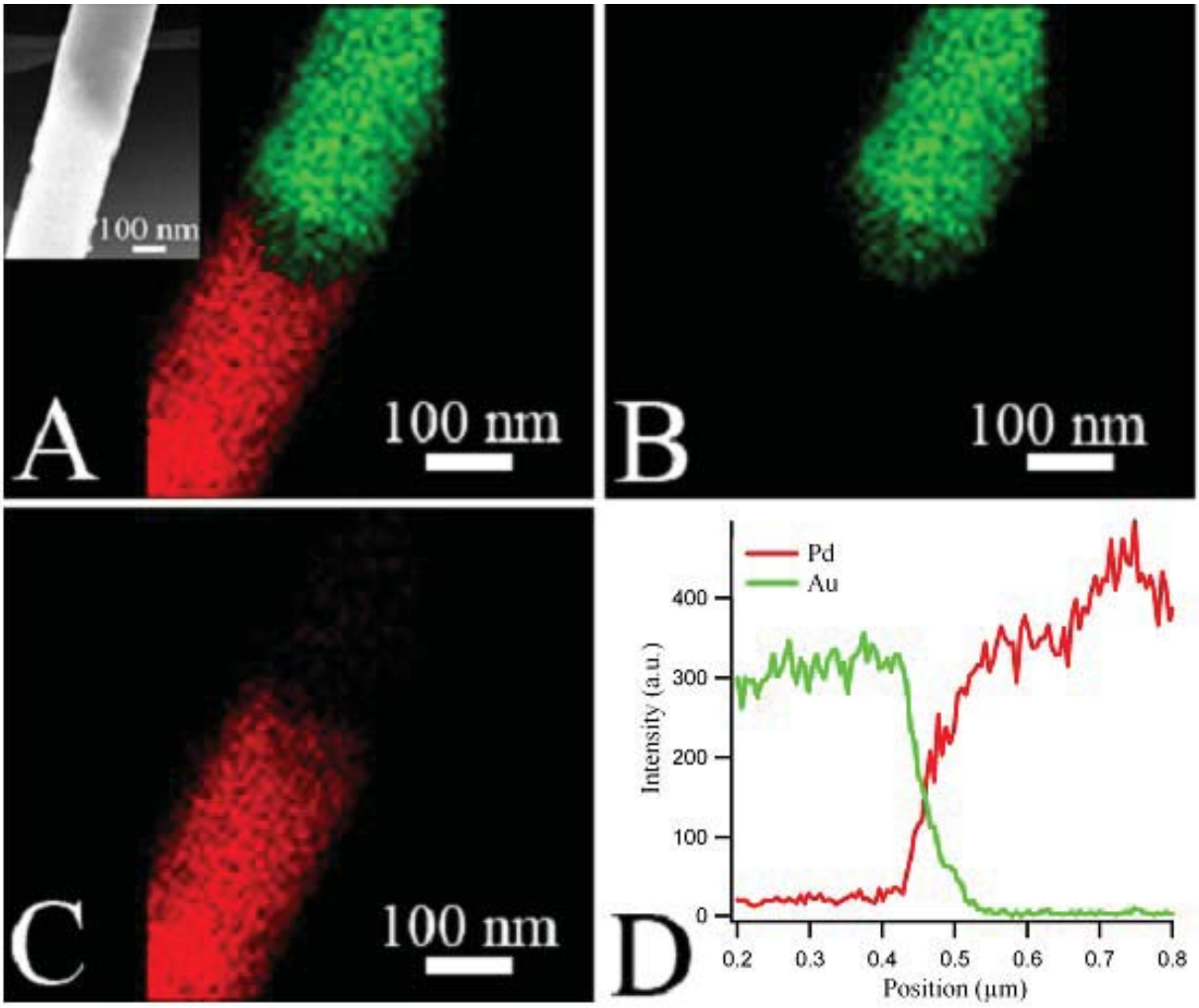

Figure 9. EDAX map of the combined Pd and Au-L edge signals (A) and HAADF (inset) data are shown of the interfacial region between the Pd and Au segments of a representative Pd/Au segmented nanowire. EDAX maps separately highlighting the Au edge signal (B) and Pd signal (C) are also shown. The intensities of the Pd and Au EDAX signals are plotted (D) as a function of the spatial position across the interfacial region.

The distribution of elements indicates there is an extremely low degree of Pd alloying across the majority region of the Au subunit, which can be visually proven by the associated mapping data (Figure 9a-c) as well as a quantitative line scan (Figure 9d). Similarly, alloying of Au within the Pd subunit is also not detectable. This distribution pattern is completely in agreement with the HAADF image, shown as an inset to Figure 9a. The shaded area, which is the Au subunit, correlates well with the Au EDAX map in Figure 9b. Hence, this result further confirms the purity of each subunit.

The interface between the two subunits, however, exhibited a relatively high degree of mixing throughout a 75-100 nm region, which comprises less than 2% of the total nanowire length. The phenomenon is possibly due to an "interdigitation" effect of both subunits. Upon completion of the first step of the experiment, the Pd subunit was terminated with an uneven surface facing the metal precursor half-cell. Elemental Au nucleated in an irregular, interdigitative manner on the existing Pd subunit, thereby resulting in a less controlled mixing of the elements at the interface region. Nevertheless, by contrast with electrodeposited nanostructures,[60] our electroless synthesized nanowires achieved a higher degree of subunit purity with a considerably shortened interdigitated interface region.

In conclusion, based on the structural and chemical characterization of our as-prepared nanowires, we can safely assert that our electroless U-tube synthesized Pd/Au nanowires achieved high elemental purity at each individual level, with a comparatively short interdigitated intersection region. The Pd subunit possesses a highly-ordered crystalline structure, whereas the Au subunit maintains a polycrystalline structure that is more ordered than that of analogous electrodeposited Au nanowires.[92,93] All of the above results collectively demonstrate our success in maintaining both purity and crystallinity during synthesis, which further validates our

electroless U-tube synthetic methodology.

3.3. Applications of As-Prepared Pd/Au Nanowires as Effective Electrocatalysts and Nanomotors.

After confirmation of our electroless synthetic methodology, we further examined the potential of our as-synthesized Pd/Au nanowires in achieving decent performance in practical multifunctional applications such as electrocatalysis and as nanoscale motor systems. First, we examined the electrocatalytic performance of 1:1 Pd/Au nanowires for the ORR, utilizing the thin-layer rotating disk electrode method (RDE).[88] CVs collected from the Pd/Au and elemental Pd nanowires between 0 and 1.6 V are shown in Figure 10, exhibiting prominent features associated with hydrogen adsorption and desorption (H_{ads}) at the 0.1 – 0.4 V region as well as oxide formation in the 0.5 – 1.0 V region.

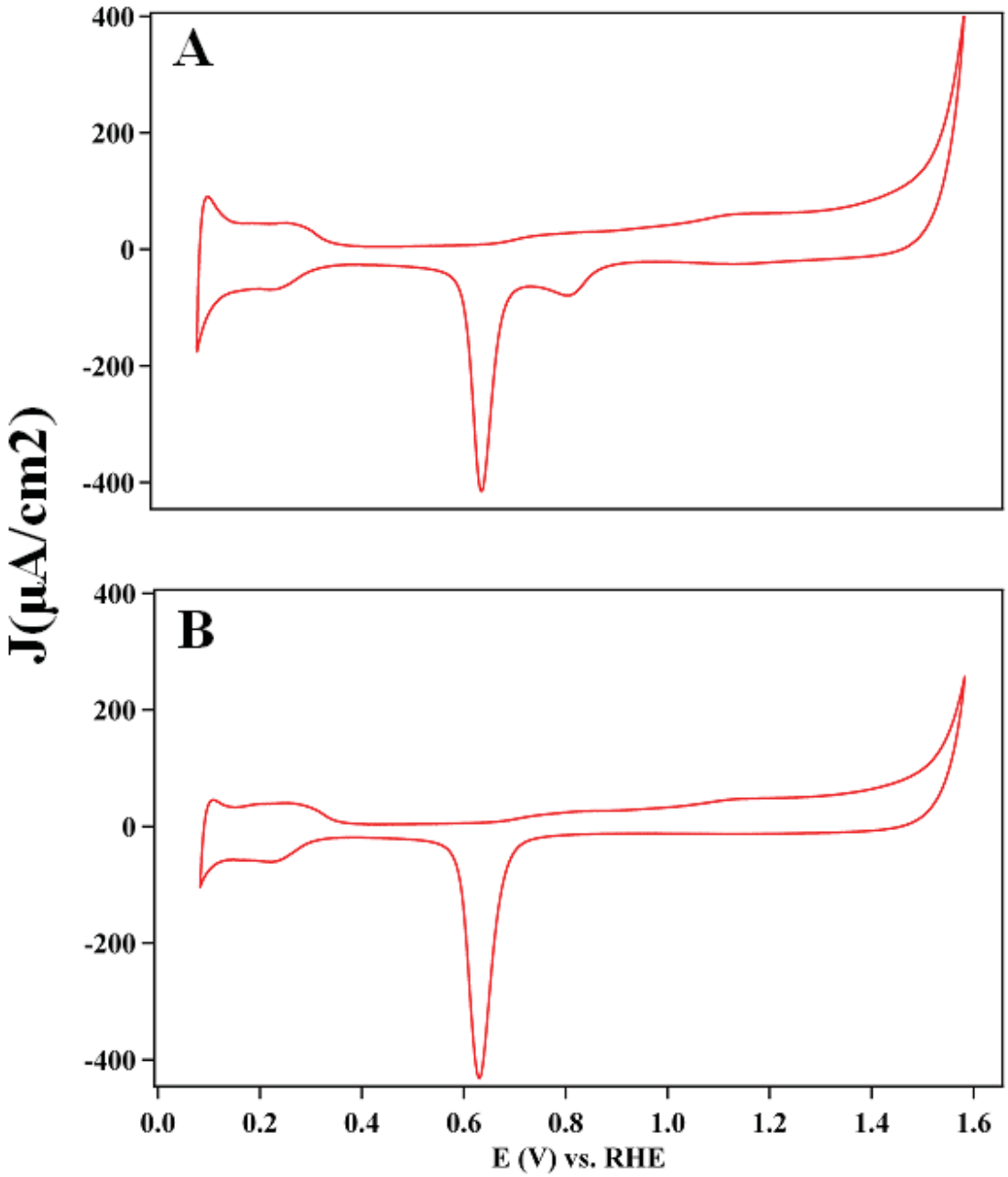

Figure 10. Cyclic voltammograms obtained from Pd/Au nanowires (A) and elemental Pd nanowires (B) obtained in deoxygenated 0.1 M $HClO_4$.

The H_{ads} performance of our as-prepared Pd/Au nanowires is confirmed by the peaks in the reduction region, which are analogous to the elemental Pd performance. A profound effect of the presence of Au segments in the Pd/Au nanowire is revealed by the peaks associated with the

surface oxide reduction region. In the case of elemental Pd (Figure 10b), the single sharp cathodic peak localized at 0.63 V is readily assigned to the reduction of oxide species adsorbed onto the active Pd surface sites. In the case of the Pd/Au species, the sharp peak at 0.65 V is accompanied by a second peak localized at 0.81 V, which can be readily assigned to the reduction of oxide species adsorbed onto the Pd-Au pair sites[94,95] and can be attributed not only to the pair sites present in the Pd-Au interfacial region but also to the minimal quantity of Pd present in the Au subunit. Interestingly, in addition to the sharp 0.65 V Pd peak and 0.81 V Au peak, the Pd/Au CV displays broader cathodic peaks at 1.13 V. This 1.13 V cathodic peak can be readily attributed to the reduction of weakly adsorbed oxide species on elemental Au active sites by the relatively inert Au subunit.

To further characterize the nature of the Pd and Au active sites present on our segmented nanowires, we utilized carbon monoxide (CO) as a probe molecule to examine their availability and role in determining the performance of Pd/Au nanowires towards CO stripping. The CO stripping voltammograms for Pd/Au and elemental Pd nanowires are shown in Figure 11.

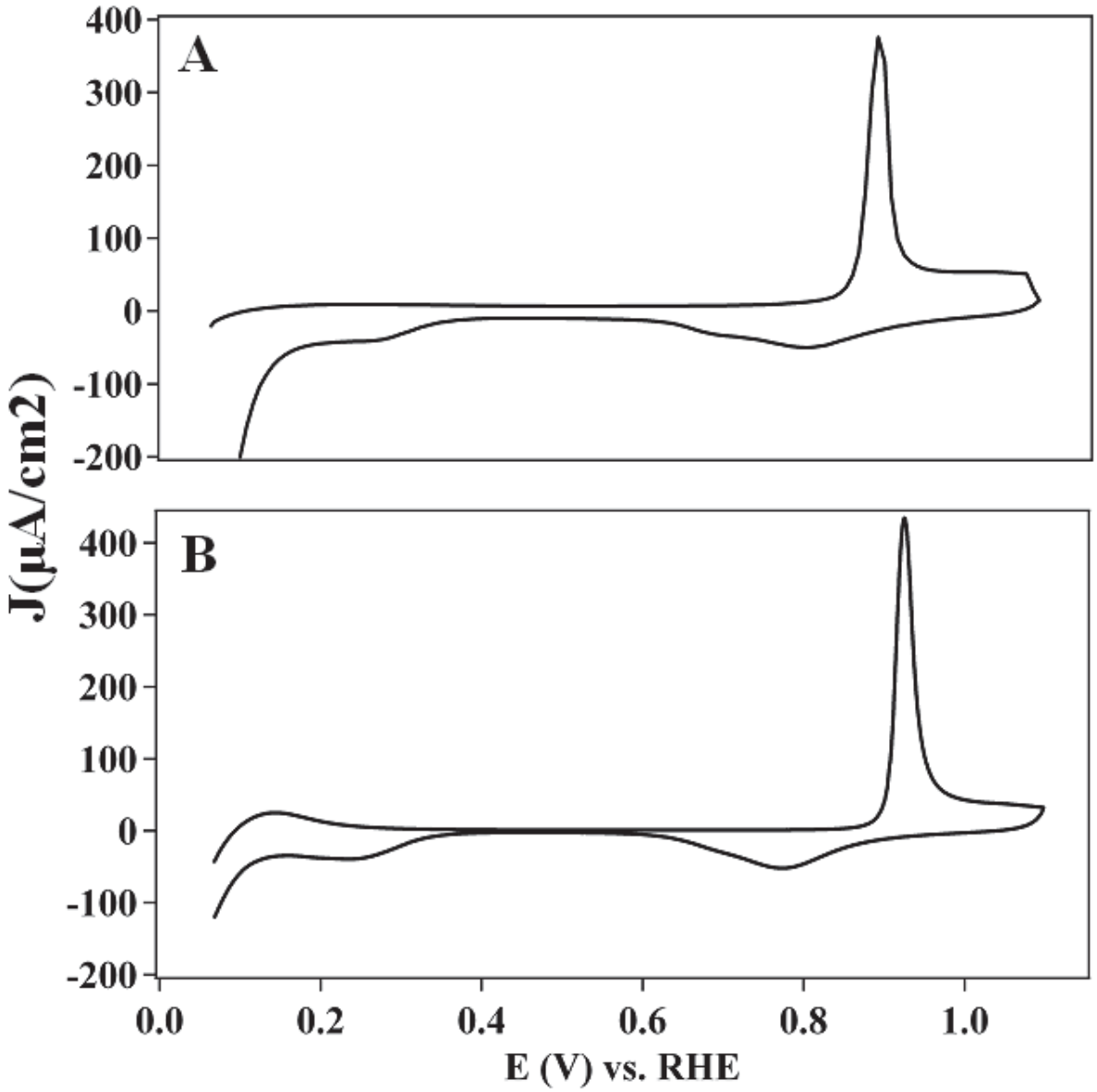

Figure 11. CO stripping voltammograms obtained from Pd/Au nanowires (A) and elemental Pd nanowires (B) obtained in deoxygenated 0.1 M $HClO_4$.

Not surprisingly, the Pd subunit (Figure 11a) displays a single sharp anodic peak at 0.890 V, consistent with CO stripping from the homogeneous Pd active sites present at the surface of the elemental nanowire (0.925 V, Figure 11b). Although it is difficult to explain the noteworthy shifts in the CO stripping peak potential of the Pd/Au nanowires, the combined effects of the bimetallic

pair sites at the interface[67-69] and the inherent electronic interactions between the segments[34,89,96,97] previously observed in these systems likely explain the significantly weakened interaction with CO.

We have also examined the inherent performance of these nanostructures towards the electrocatalytic reduction of oxygen in acidic media. Polarization curves obtained from the Pd/Au nanowires in oxygen saturated 0.1 M $HClO_4$ electrolyte (Figure 12) reveal the performance of the Pd/Au nanowires.

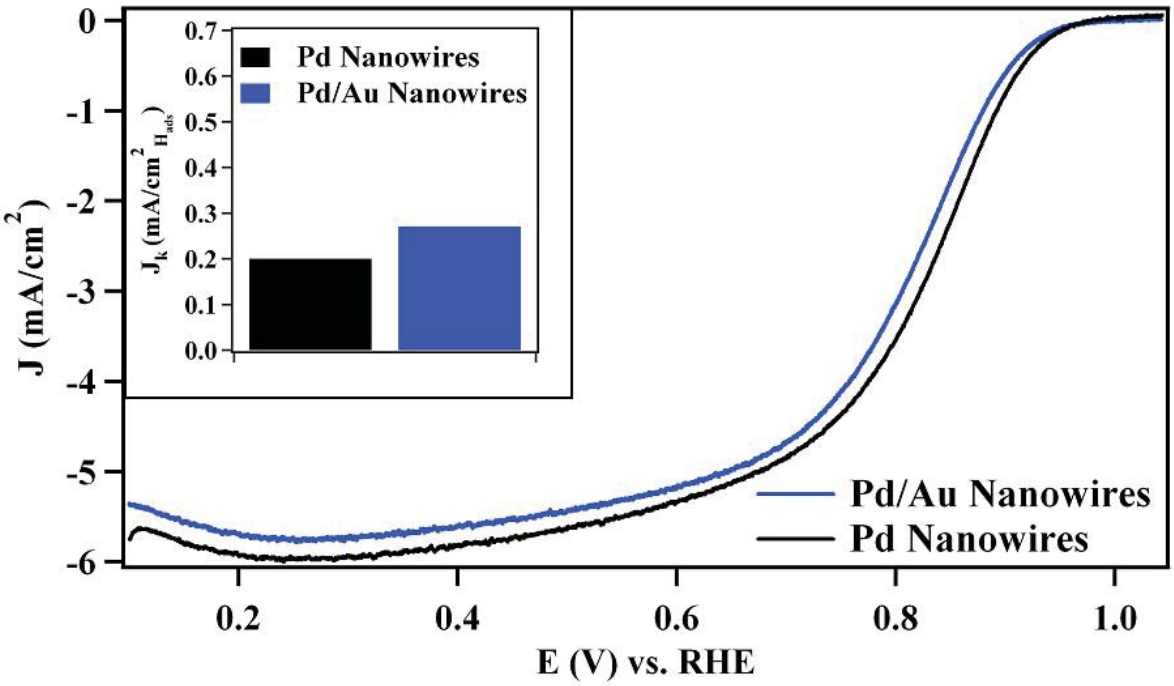

Figure 12. Polarization curves (anodic sweep direction) obtained from Pd/Au nanowires (blue) and elemental Pd nanowires (black) in an oxygen-saturated 0.1 M $HClO_4$ solution at 1600 rpm and 20°C. The measured surface activity normalized kinetic currents (specific activities) at 0.9 V are shown as an inset.

In this case, the electrochemically active surface area of the Pd subunit is determined from the integrated H_{ads} charge. As expected, the presence of the Pd subunit was responsible for the

majority of hydrogen adsorption; the elemental gold active sites do not undergo hydrogen adsorption and maintain nearly undetectable levels of oxygen reduction in acidic media.[34,89] Since the gold segment is essentially electrochemically inert under these conditions, the measured specific activity of the Pd/Au nanowires is solely related to the nature of the Pd active sites present on the Pd sub-unit. Therefore, it is not unanticipated that the measured specific activity (0.27 mA/cm^2) of the Pd active sites agrees very well with the corresponding value obtained from analogous active sites on elemental Pd nanowires (0.20 mA/cm^2). The slight but measurable enhancement in the performance of the Pd active sites in this case collectively may arise from the presence of Pd-Au bimetallic sites present at the interface[34,89] as well as from advantageous electronic effects,[96,97] which are well characterized in Pd-Au systems. Collectively, the electrocatalytic performance of these nanostructures confirms that Pd and Au active sites are not only present but also retain a catalytic performance potential, analogous to or even enhanced as compared with their bulk elemental counterparts.

In the broader sense, the electrocatalysis data obtained from the Pd/Au nanowires collectively indicate that the as-prepared segmented Pd/Au nanowires maintain Pd and Au active sites with electrochemical behavior consistent with that of their elemental counterparts. Furthermore, these results clearly demonstrate that the segmented nanowire architecture allows for the mutual presence of two types of distinctive active sites to be present on the same nanowire simultaneously. This observed catalytic multi-functionality is uncommon, and in theory, may render a single nanostructure capable of catalyzing more than one electrochemical reaction with tunable, targeted specificity.

In addition to the demonstration of their outstanding electrochemical and catalytic properties, we also examined as-prepared Pd/Au segmented nanowires as catalytic nanomotors.

Several plausible reasons are revealed in the literature to explain the locomotion mechanism of nanomotors. These include (i) self-diffusiophoresis due to concentration gradients in solute,[98] (ii) an interfacial tension gradient mechanism in which oxygen produced in the reaction lowered the interfacial tension between the aqueous solution and the gas-coated nanowires,[45,47,99] and (iii) a Brownian ratchet mechanism in which the oxygen evolved on one segment decreases the local viscosity.[46,50] A more recent hypothesis attributed the observed behavior to oxygen bubbles' evolution (e.g. bubble-induced propulsion) from the nanowire surface coupled with a model based on related gravitational forces, which treat the nanowires in the context of 3D space.[100]

Nonetheless, the most common and accepted rationale for the self-propulsion of bimetallic catalytic motors was put forth by Mallouk and co-workers,[45,58] who suggested that the inherent locomotion in the presence of H_2O_2 results from a so-called self-electrophoresis process, namely a migration of the particle in an electric field generated by the nanowire itself as a result of its inherent compositional asymmetry. Specifically, it is believed that (a) the electrochemical oxidation and decomposition of peroxide to generate protons, electrons, and O_2, as well as (b) the corresponding, complementary reduction reaction involving the combination of protons, electrons, peroxide, and O_2 to produce water at the surfaces of the nanowire are separately catalyzed by Pd and Au subunits present at either end of the nanowire. Wang et al. [51] found that the redox equations describing H_2O_2 oxidation and reduction at the terminals of these bimetallic nanowires can be written as Equations 4 through 6.

Equation 4. Oxidation at the anodic subunit.

$$2H_2O_2(aq) \rightarrow 2O_2(g) + 4H^+(aq) + 4e^-$$

Equation 5. Reduction at the cathodic subunit.

$$O_2(g) + 4H^+(aq) + 4e^- \rightarrow 2H_2O(l)$$

Equation 6. Overall reduction reaction.

$2H_2O_2(aq) \rightarrow O_2(g) + 2H_2O(l)$

Since these electrochemical processes are spatially separated, in order to conserve overall charge, the corresponding mass transport of water and protons from the anode subunit to cathode subunit results in the increased motion of the nanowire through the aqueous media. It is as if the nanowire behaved as a short-circuited galvanic cell, driving a net migration of protons in the surrounding solution from the anode to the cathode.[101] The net fluid motion thereby results in locomotion of the nanowires in the direction of the anode. Not surprisingly, this self-electrophoresis process can lead to nanowire velocities that far exceed those typically observed in pure water.[2,22,41,42,44-64,101]

Inspired by Sen's research,[41,42,44-61,63,64] we employed the H_2O_2-driven nanomotor system and video-recorded the movements for further quantitative analysis. Figure 13 demonstrates the relationship between the concentration of H_2O_2 and the velocity of the as-prepared Pd/Au nanowires.

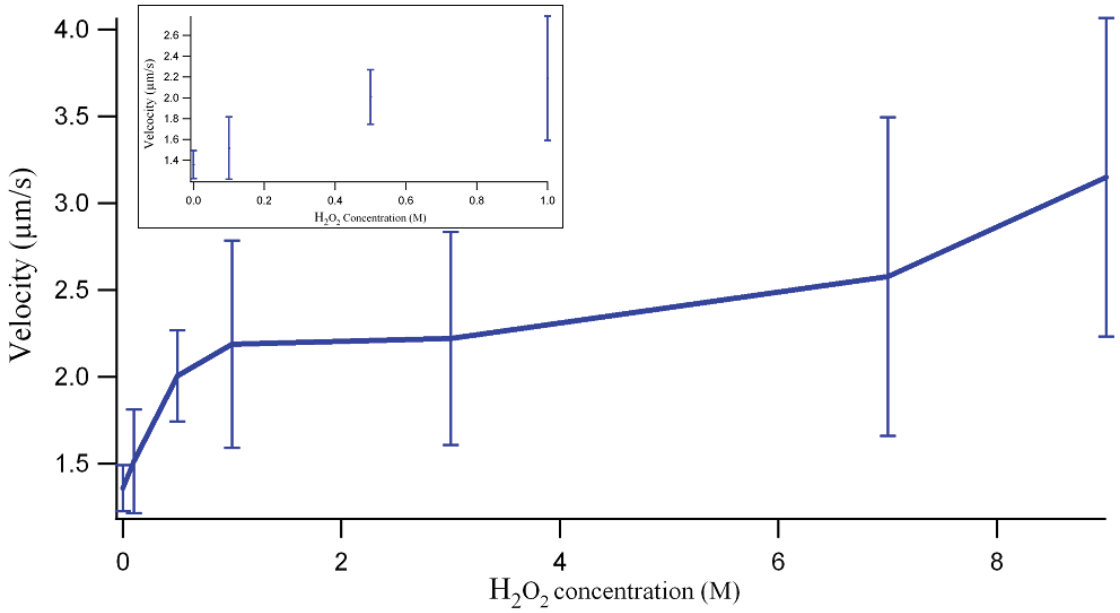

Figure 13. The velocity of Pd/Au nanowires dispersed into an aqueous solution as a function of the concentration of H_2O_2 present. The region between 0 and 1 M is expanded for the sake of clarity and is shown as an inset.

The behavior of the nanowires in deionized water serving as a control reveals that the nanowires maintain relatively low velocities (1.36 ± 0.13 μm/sec) without observable gas formation. As a comparison, a 1:1 mixture of H_2O_2 and DI water without any nanowire content exhibited little if any significant quantity of gas bubble formation throughout a 30 minute period of time. According to Wang et al.,[51] the main mechanism accounting for nanowire movement is characterized by an increased nanowire velocity as well as O_2 gas formation as a byproduct (Equation 6). Therefore, gas formation is an expected phenomenon along with a measurably increased velocity.

The as-prepared Pd/Au nanowires are susceptible and responsive to the presence of H_2O_2. The study of the as-prepared nanowires' locomotion in DI water suggests that they maintain Brownian motion in such conditions. The presence of H_2O_2 drastically alters the movements of

the nanowires. As indicated in Figure 13, specifically, alterations in the H_2O_2 concentration can induce corresponding modifications in the velocities of both types of nanowires. In a 0.1 M H_2O_2 concentration environment, Pd/Au nanowires attained velocities of 0.152 ± 0.30 μm/sec and maintained a steady increasing trend up to a 3 M H_2O_2 concentration. Furthermore, a significant amount of gas bubbles was generated, immediately following the initial contact of H_2O_2 with the Pd/Au nanowire suspensions. This gas-forming phenomenon was observed in all reaction mixtures containing nanowires with H_2O_2 at all concentrations tested. As compared with the non-gas-forming H_2O_2/DI water mixture, the formation of gas bubbles in this reaction mixture indicates an ongoing process of H_2O_2 reduction. Simultaneously, an increased nanowire velocity was consistent with the self-electrophoresis mechanism, alluded to previously.

Specifically, Pd/Au nanowires exhibited a highlighted responsiveness to H_2O_2 concentration, as revealed by its corresponding velocity. At lower H_2O_2 concentrations (< 3 M), the nanowire velocity increases in a linear trend. As H_2O_2 concentrations peak (from 7 to 9 M), the relative level of responsiveness decreases, resulting in a slower rate of increment of velocity. In 9 M H_2O_2 solutions, the average velocities of Pd/Au nanowires attained values of 3.15 ± 0.92 μm/sec. This phenomenon is possibly due to a gradual saturation of reduction processes at both subunits, which can lead to a quantitatively maximized and relatively steady electron supply available for self-electrophoresis. Interestingly, the velocity of our as-prepared Pd/Au nanowires is significantly lower than results in 1.67 M H_2O_2 solution (Pd/Au = 15.3 ± 2.0 μm/sec).[51] Our data are in agreement with a previous prediction, in which it was postulated that longer nanowires tend to travel at slower velocities as compared with shorter nanowires. From a physical perspective, extra torque is needed to move nanowires that possess larger surface areas and volumes. With an average length up to 8.16 ± 1.35 μm, the Pd/Au nanowires are significantly

longer than the ones reported by a previous group (~ 2 μm).[51] Therefore, at a given concentration of H_2O_2, longer as-synthesized Pd/Au nanowires tend to move slower than their shorter counterparts.

The pathway of the nanowire movement provides additional information regarding its chemotaxis behavior. Figure 14 exhibits a comparison of representative sample trajectories of Pd/Au nanowires in the presence of DI water and 9 M H_2O_2, respectively.

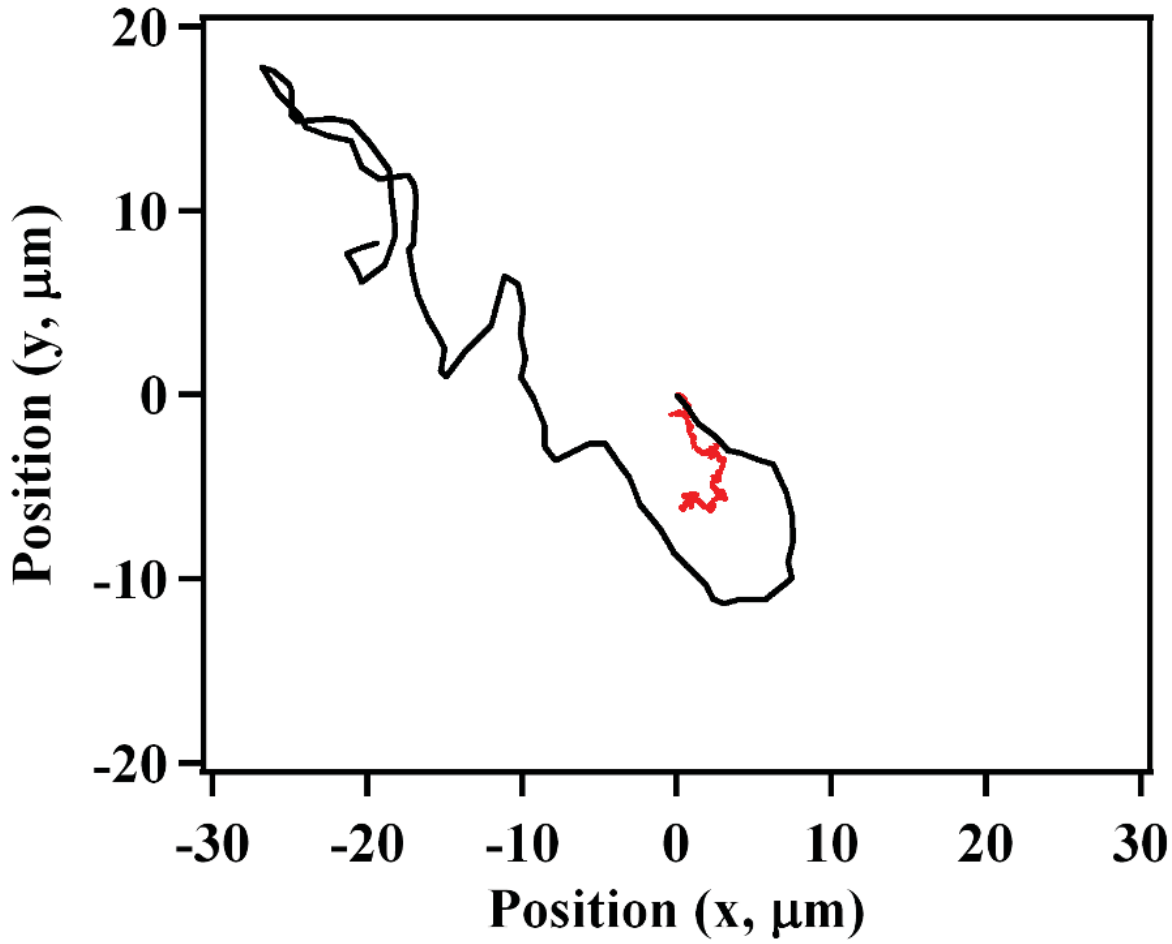

Figure 14. Graphical depiction of the 2D trajectory (measured by confocal microscopy), traced out by Pd/Au nanowires in 9 M H_2O_2 (black trace) and pure water (red). The nanowire motion is

captured over a period of 20 s with the initial position ('t' = 0 s) of the nanowire, arbitrarily placed at (0, 0).

The exhibited plot indicates that the selected nanowire was moving somewhat erratically in the reagent solution, especially in water. In a prior report,[51] in the Pd/Au nanowire system, electron flow occurs from the Pd subunit to the Au subunit, thereby resulting in the Pd subunit 'directing' movement. Due to limitations of instrumentation, we are currently unable to confirm the suggested directionality while simultaneously identifying the subunit compositions which are at the root of the observed movement. Nevertheless, with our currently applied methodology, we are able to show that the directionalities of the nanowires were maintained throughout time, an assertion supported by the fact that one subunit of the nanowire always tends to preferentially guide the observed movement.

Although there is a high degree of directionality to the motion in H_2O_2, the observed pathways are not necessarily linear, a fact which may arise from the slight curvature of the as-prepared Pd/Au nanowire that is readily apparent in the SEM images (Figure 7). A recent study on a copper/platinum 1D nanomotor system[60] has indicated that the curvature of the nanowire can influence both the hydrodynamic flow of water over the nanowire surface as well as the localized drag coefficient, thereby accounting for the somewhat erratic trajectories observed. Additional optimization of these as-prepared nanowires (including but not limited to manipulations of their surface roughness),[64] which is beyond the scope of this report, may lead to the formation of more morphologically perfected 1D morphologies and hence, the possibility of more predictable and faster swimming patterns in H_2O_2 solution.

Chapter IV. Conclusions.

Multifunctional nanostructures possess a broad range of applications and potentials in systems such as catalysis, sensing, information storage, and more recently, nano-transportation. Bimetallic segmented nanowires represent an exciting structural paradigm for preparing multifunctional nanostructures applicable in the above mentioned systems. However, the widespread use of these valuable nanostructures has been hindered by the lack of efficient, scalable, and sustainable methods for their reliable preparation. In this report, our U-tube-based electroless synthesis of Pd/Au segmented nanowires was presented as a viable protocol for an ambient, surfactantless, template-based approach for the preparation of segmented noble metal nanowires. Via simple chemical reduction processes, the as-prepared Pd/Au nanowires confirmed our ability to manipulate the relative segment lengths over a broad range; structural characterization further indicated that the individual segments maintain a high degree of purity with minimal alloying. In addition, the generation of a sharp, well-defined interface as well as the production of a highly ordered segmental crystalline structure all collectively suggest that our methodology for preparing multi-segmented nanowires is not only straightforward and cost-effective, but also unburdened by the potential complexities associated with either electrodeposition or physical vapor deposition processes.

Examination of the performance of the as-prepared Pd/Au nanowires as electrocatalysts and nanomotors further demonstrates their potential for applications in practical multifunctional systems. Careful electrochemical analysis of the Pd/Au nanowires reveals that the individual nanostructures maintain dual Pd and Au active sites with electrochemical properties that are commensurate with their elemental counterparts. The electrocatalytic reduction of oxygen by these segmented systems further shows that these dual active sites are not only present but also

catalytically active. These results collectively render our segmented nanowires as excellent candidates for catalyzing multiple reactions with reasonable chemical specificity through a single nanostructure. In addition, a study of the locomotion behavior of the Pd/Au nanowires in H_2O_2 solutions demonstrates a H_2O_2 concentration-dependent velocity increment, which confirms that the as-prepared Pd/Au nanowires are sensitive and responsive to peroxide concentrations as low as 0.1 M. Furthermore, this result highlights the promising application of our as-prepared nanowires as autonomous nanomotors with the potential of acting as carriers for the transportation of cargo.[54,62] In conclusion, our simple and cost-effective synthetic method is capable of generating versatile nanowires applicable for a wide variety of functional roles without the need for either additional processing or purification steps.

References

(1) Xia, Y. N.; Yang, P. D.; Sun, Y. G.; Wu, Y. Y.; Mayers, B.; Gates, B.; Yin, Y. D.; Kim, F.; Yan, Y. Q. *Advanced Materials* **2003**, *15*, 353.

(2) Kline, T. R.; Tian, M.; Wang, J.; Sen, A.; Chan, M. W. H.; Mallouk, T. E. *Inorganic Chemistry* **2006**, *45*, 7555.

(3) Chen, J.; Wiley, B. J.; Xia, Y. *Langmuir* **2007**, *23*, 4120.

(4) Mao, Y.; Park, T.-J.; Zhang, F.; Zhou, H.; Wong, S. S. *Small* **2007**, *3*, 1122.

(5) Tiano, A. L.; Koenigsmann, C.; Santulli, A. C.; Wong, S. S. *Chemical Communications* **2010**, *46*, 8093.

(6) Murphy, C. J.; San, T. K.; Gole, A. M.; Orendorff, C. J.; Gao, J. X.; Gou, L.; Hunyadi, S. E.; Li, T. *Journal of Physical Chemistry B* **2005**, *109*, 13857.

(7) Murphy, C. J.; Sau, T. K.; Gole, A.; Orendorff, C. J. *Mrs Bulletin* **2005**, *30*, 349.

(8) Chen, Z.; Waje, M.; Li, W.; Yan, Y. *Angewandte Chemie-International Edition* **2007**, *46*, 4060.

(9) Zijlstra, P.; Chon, J. W. M.; Gu, M. *Nature* **2009**, *459*, 410.

(10) Stoermer, R. L.; Cederquist, K. B.; McFarland, S. K.; Sha, M. Y.; Penn, S. G.; Keating, C. D. *Journal of the American Chemical Society* **2006**, *128*, 16892.

(11) Brunker, S. E.; Cederquist, K. B.; Keating, C. D. *Nanomedicine* **2007**, *2*, 695.

(12) Sioss, J. A.; Stoermer, R. L.; Sha, M. Y.; Keating, C. D. *Langmuir* **2007**, *23*, 11334.

(13) Cederquist, K. B.; Dean, S. L.; Keating, C. D. *Wiley Interdisciplinary Reviews-Nanomedicine and Nanobiotechnology* **2010**, *2*, 578.

(14) Keating, C. D.; Natan, M. J. *Advanced Materials* **2003**, *15*, 451.

(15) Lee, K.-S.; El-Sayed, M. A. *Journal of Physical Chemistry B* **2006**, *110*, 19220.

(16) Tong, L.; Wei, Q.; Wei, A.; Cheng, J.-X. *Photochemistry and Photobiology* **2009**, *85*, 21.

(17) Pena, D. J.; Mbindyo, J. K. N.; Carado, A. J.; Mallouk, T. E.; Keating, C. D.; Razavi, B.; Mayer, T. S. *Journal of Physical Chemistry B* **2002**, *106*, 7458.

(18) Reiss, B. D.; Freeman, R. G.; Walton, I. D.; Norton, S. M.; Smith, P. C.; Stonas, W. G.; Keating, C. D.; Natan, M. J. *Journal of Electroanalytical Chemistry* **2002**, *522*, 95.

(19) Nicewarner-Pena, S. R.; Carado, A. J.; Shale, K. E.; Keating, C. D. *Journal of Physical Chemistry B* **2003**, *107*, 7360.

(20) Stoermer, R. L.; Keating, C. D. *Journal of the American Chemical Society* **2006**, *128*, 13243.

(21) Dean, S. L.; Stapleton, J. J.; Keating, C. D. *Langmuir* **2010**, *26*, 14861.

(22) Wang, J. *Chemphyschem* **2009**, *10*, 1748.

(23) Zhao, W.; Brook, M. A.; Li, Y. *Chembiochem* **2008**, *9*, 2363.

(24) Zheng, G. F.; Patolsky, F.; Cui, Y.; Wang, W. U.; Lieber, C. M. *Nature Biotechnology* **2005**, *23*, 1294.

(25) Patolsky, F.; Zheng, G.; Lieber, C. M. *Nanomedicine* **2006**, *1*, 51.

(26) Patolsky, F.; Zheng, G. F.; Lieber, C. M. *Analytical Chemistry* **2006**, *78*, 4260.

(27) Lee, J. H.; Wu, J. H.; Liu, H. L.; Cho, J. U.; Cho, M. K.; An, B. H.; Min, J. H.; Noh, S. J.; Kim, Y. K. *Angewandte Chemie-International Edition* **2007**, *46*, 3663.

(28) Creran, B.; Yan, B.; Moyano, D. F.; Gilbert, M. M.; Vachet, R. W.; Rotello, V. M. *Chemical Communications* **2012**, *48*, 4543.

(29) Koenigsmann, C.; Zhou, W.-p.; Adzic, R. R.; Sutter, E.; Wong, S. S. *Nano Letters*

2010, *10*, 2806.

(30) Koenigsmann, C.; Santulli, A. C.; Gong, K.; Vukmirovic, M. B.; Zhou, W.-p.; Sutter, E.; Wong, S. S.; Adzic, R. R. *Journal of the American Chemical Society* **2011**, *133*, 9783.

(31) Koenigsmann, C.; Santulli, A. C.; Sutter, E.; Wong, S. S. *Acs Nano* **2011**, *5*, 7471.

(32) Koenigsmann, C.; Wong, S. S. *Energy & Environmental Science* **2011**, *4*, 1161.

(33) Zhou, W.-P.; Li, M.; Koenigsmann, C.; Ma, C.; Wong, S. S.; Adzic, R. R. *Electrochimica Acta* **2011**, *56*, 9824.

(34) Koenigsmann, C.; Sutter, E.; Adzic, R. R.; Wong, S. S. *The Journal of Physical Chemistry C* **2012**, *116*, 15297.

(35) Zhou, H.; Zhou, W.-p.; Adzic, R. R.; Wong, S. S. *Journal of Physical Chemistry C* **2009**, *113*, 5460.

(36) Antolini, E.; Perez, J. *Journal of Materials Science* **2011**, *46*, 4435.

(37) Morozan, A.; Jousselme, B.; Palacin, S. *Energy & Environmental Science* **2011**, *4*, 1238.

(38) Patete, J. M.; Peng, X.; Koenigsmann, C.; Xu, Y.; Karn, B.; Wong, S. S. *Green Chemistry* **2011**, *13*, 482.

(39) Reich, D. H.; Tanase, M.; Hultgren, A.; Bauer, L. A.; Chen, C. S.; Meyer, G. J. *Journal of Applied Physics* **2003**, *93*, 7275.

(40) Sarkar, J.; Khan, G. G.; Basumallick, A. *Bulletin of Materials Science* **2007**, *30*, 271.

(41) Hong, Y.; Blackman, N. M. K.; Kopp, N. D.; Sen, A.; Velegol, D. *Physical Review Letters* **2007**, *99*, 178103.

(42) van den Heuvel, M. G. L.; Dekker, C. *Science* **2007**, *317*, 333.

(43) Mavroidis, C.; Dubey, A.; Yarmush, M. L. *Annual Review of Biomedical Engineering* **2004**, *6*, 363.

(44) Schliwa, M.; Woehlke, G. *Nature* **2003**, *422*, 759.

(45) Paxton, W. F.; Sundararajan, S.; Mallouk, T. E.; Sen, A. *Angewandte Chemie-International Edition* **2006**, *45*, 5420.

(46) Wang, J. *Acs Nano* **2009**, *3*, 4.

(47) Paxton, W. F.; Kistler, K. C.; Olmeda, C. C.; Sen, A.; St Angelo, S. K.; Cao, Y. Y.; Mallouk, T. E.; Lammert, P. E.; Crespi, V. H. *Journal of the American Chemical Society* **2004**, *126*, 13424.

(48) Kline, T. R.; Paxton, W. F.; Mallouk, T. E.; Sen, A. *Angewandte Chemie-International Edition* **2005**, *44*, 744.

(49) Paxton, W. F.; Sen, A.; Mallouk, T. E. *Chemistry-a European Journal* **2005**, *11*, 6462.

(50) Dhar, P.; Fischer, T. M.; Wang, Y.; Mallouk, T. E.; Paxton, W. F.; Sen, A. *Nano Letters* **2006**, *6*, 66.

(51) Wang, Y.; Hernandez, R. M.; Bartlett, D. J., Jr.; Bingham, J. M.; Kline, T. R.; Sen, A.; Mallouk, T. E. *Langmuir* **2006**, *22*, 10451.

(52) Ibele, M. E.; Wang, Y.; Kline, T. R.; Mallouk, T. E.; Sen, A. *Journal of the American Chemical Society* **2007**, *129*, 7762.

(53) Demirok, U. K.; Laocharoensuk, R.; Manesh, K. M.; Wang, J. *Angewandte Chemie-International Edition* **2008**, *47*, 9349.

(54) Sundararajan, S.; Lammert, P. E.; Zudans, A. W.; Crespi, V. H.; Sen, A. *Nano Letters* **2008**, *8*, 1271.

(55) Balasubramanian, S.; Kagan, D.; Manesh, K. M.; Calvo-Marzal, P.; Flechsig, G.-U.; Wang, J. *Small* **2009**, *5*, 1569.

(56) Calvo-Marzal, P.; Manesh, K. M.; Kagan, D.; Balasubramanian, S.; Cardona, M.; Flechsig, G.-U.; Posner, J.; Wang, J. *Chemical Communications* **2009**, 4509.

(57) Ibele, M.; Mallouk, T. E.; Sen, A. *Angewandte Chemie-International Edition* **2009**, *48*, 3308.

(58) Wang, Y.; Fei, S.-t.; Byun, Y.-M.; Lammert, P. E.; Crespi, V. H.; Sen, A.; Mallouk, T. E. *Journal of the American Chemical Society* **2009**, *131*, 9926.

(59) Hong, Y.; Velegol, D.; Chaturvedi, N.; Sen, A. *Physical Chemistry Chemical Physics* **2010**, *12*, 1423.

(60) Liu, R.; Sen, A. *Journal of the American Chemical Society* **2011**, *133*, 20064.

(61) Pak, O. S.; Gao, W.; Wang, J.; Lauga, E. *Soft Matter* **2011**, *7*, 8169.

(62) Baraban, L.; Tasinkevych, M.; Popescu, M. N.; Sanchez, S.; Dietrich, S.; Schmidt, O. G. *Soft Matter* **2012**, *8*, 48.

(63) Campuzano, S.; Orozco, J.; Kagan, D.; Guix, M.; Gao, W.; Sattayasamitsathit, S.; Claussen, J. C.; Merkoci, A.; Wang, J. *Nano Letters* **2012**, *12*, 396.

(64) Gao, W.; Sattayasamitsathit, S.; Wang, J. *Chemical Record* **2012**, *12*, 224.

(65) Gao, W.; Kagan, D.; Pak, O. S.; Clawson, C.; Campuzano, S.; Chuluun-Erdene, E.; Shipton, E.; Fullerton, E. E.; Zhang, L.; Lauga, E.; Wang, J. *Small* **2012**, *8*, 460.

(66) Hurst, S. J.; Payne, E. K.; Qin, L. D.; Mirkin, C. A. *Angewandte Chemie-International Edition* **2006**, *45*, 2672.

(67) Liu, F.; Lee, J. Y.; Zhou, W. J. *Advanced Functional Materials* **2005**, *15*, 1459.

(68) Liu, F.; Lee, J. Y.; Zhou, W. *Journal of the Electrochemical Society* **2006**, *153*,

A2133.

(69) Liu, F.; Lee, J. Y.; Zhou, W. J. *Small* **2006**, *2*, 121.

(70) Shaijumon, M. M.; Ou, F. S.; Ci, L.; Ajayan, P. M. *Chemical Communications* **2008**, 2373.

(71) Shen, G.; Chen, P.-C.; Ryu, K.; Zhou, C. *Journal of Materials Chemistry* **2009**, *19*, 828.

(72) Sun, Y. G.; Graff, R. A.; Strano, M. S.; Rogers, J. A. *Small* **2005**, *1*, 1052.

(73) Wagner, R. S.; Ellis, W. C. *Applied Physics Letters* **1964**, *4*, 89.

(74) Akhtar, J.; Akhtar, M.; Malik, M. A.; O'Brien, P.; Raftery, J. *Journal of the American Chemical Society* **2012**, *134*, 2485.

(75) LaLonde, A. D.; Norton, M. G.; McIlroy, D. N.; Zhang, D. Q.; Padmanabhan, R.; Alkhateeb, A.; Han, H. M.; Lane, N.; Holman, Z. *Journal of Materials Research* **2005**, *20*, 549.

(76) Park, S.; Hong, C.; Kang, J.; Cho, N.; Lee, C. *Current Applied Physics* **2009**, *9*, S230.

(77) Aharonovich, I.; Tamir, S.; Lifshitz, Y. *Nanotechnology* **2008**, *19*.

(78) Martin, C. R. *Science* **1994**, *266*, 1961.

(79) Dai, H. J.; Wong, E. W.; Lu, Y. Z.; Fan, S. S.; Lieber, C. M. *Nature* **1995**, *375*, 769.

(80) Hulteen, J. C.; Martin, C. R. *Journal of Materials Chemistry* **1997**, *7*, 1075.

(81) Zhang, F.; Mao, Y.; Park, T.-J.; Wong, S. S. *Advanced Functional Materials* **2008**, *18*, 103.

(82) Zhang, F.; Yiu, Y.; Aronson, A. C.; Wong, S. S. *Journal of Physical Chemistry C* **2008**, *112*, 14816.

(83) Etzion, M.; Blech, I. A.; Komem, Y. *Journal of Applied Physics* **1975**, *46*, 1455.

(84) Hook, G.; Lai, C.; Bastacky, J.; Hayes, T. *Scanning electron microscopy* **1980**, 27.

(85) Enders, D.; Nagao, T.; Nakayamai, T.; Aono, M. *Japanese Journal of Applied Physics Part 2-Letters & Express Letters* **2007**, *46*, L1222.

(86) Langhammer, C.; Larsson, E. M.; Kasemo, B.; Zoric, I. *Nano Letters* **2010**, *10*, 3529.

(87) Dean, J. A. *Lange's Handbook of Chemistry*; McGRAW-HILL INC.: New York, San Francisco, Washington, D.C., Auckland, Bogota, Caracas, Lisbon, London, Madrid, Mexico City, Milan, Montreal, New Delhi, San Juan, Singapore, Sydney, Tokyo, Toronto, 1992; Vol. 14.

(88) Garsany, Y.; Baturina, O. A.; Swider-Lyons, K. E.; Kocha, S. S. *Analytical Chemistry* **2010**, *82*, 6321.

(89) Koenigsmann, C.; Sutter, E.; Chiesa, T. A.; Adzic, R. R.; Wong, S. S. *Nano Letters* **2012**, *12*, 2013.

(90) Schonenberger, C.; vanderZande, B. M. I.; Fokkink, L. G. J.; Henny, M.; Schmid, C.; Kruger, M.; Bachtold, A.; Huber, R.; Birk, H.; Staufer, U. *Journal of Physical Chemistry B* **1997**, *101*, 5497.

(91) Huiqing Peng, C. K., Zhibo Tan, Stanisalus Wong **2012**.

(92) Zhang, X. Y.; Zhang, L. D.; Lei, Y.; Zhao, L. X.; Mao, Y. Q. *Journal of Materials Chemistry* **2001**, *11*, 1732.

(93) Kante, I.; Andreazza, P.; Andreazza, C.; Devers, T.; Allam, L.; Fleury, V. *Journal of Crystal Growth* **2005**, *277*, 599.

(94) Shim, J. H.; Kim, J.; Lee, C.; Lee, Y. *Chemistry of Materials* **2011**, *23*, 4694.

(95) Sarapuu, A.; Kasikov, A.; Wong, N.; Lucas, C. A.; Sedghi, G.; Nichols, R. J.; Tammeveski, K. *Electrochimica Acta* **2010**, *55*, 6768.

(96) Damjanov.A; Brusic, V. *Electrochimica Acta* **1967**, *12*, 1171.

(97) Damjanov.A; Brusic, V.; Bockris, J. O. *Journal of Physical Chemistry* **1967**, *71*, 2741.

(98) Howse, J. R.; Jones, R. A. L.; Ryan, A. J.; Gough, T.; Vafabakhsh, R.; Golestanian, R. *Physical Review Letters* **2007**, *99*.

(99) Saidulu, N. B.; Sebastian, K. L. *Journal of Chemical Physics* **2008**, *128*.

(100) Kovtyukhova, N. I. *Journal of Physical Chemistry C* **2008**, *112*, 6049.

(101) Moran, J. L.; Wheat, P. M.; Posner, J. D. *Physical Review E* **2010**, *81*.